UNCLASSIFIED

AD NUMBER

AD916925

NEW LIMITATION CHANGE

TO

Approved for public release, distribution unlimited

FROM

Distribution authorized to U.S. Gov't. agencies only; Test and Evaluation; 14 Dec 1973. Other requests shall be referred to Naval Weapons Center, China Lake, CA .

AUTHORITY

USNWC ltr, 14 May 1975

THIS PAGE IS UNCLASSIFIED

AD916925

Effect of Projectile Nose Shape on Ballistic Limit Velocity, Residual Velocity, and Ricochet Obliquity

by

Thomas W. Ipson
Rodney F. Recht
William A. Schmeling
Denver Research Institute
for the
Weapons Development Department

D D C

FEB 19 1974

E

Naval Weapons Center NWC

CHINA LAKE, CALIFORNIA ● DECEMBER 1973

ii

Naval Weapons Center

AN ACTIVITY OF THE NAVAL MATERIAL COMMAND

FOREWORD

The Chief of Naval Material Command (CNM) assigned to a group of Navy laboratories a program on Soviet ship vulnerability; one of these laboratories was the Naval Weapons Center (NWC), China Lake. Calif. As a part of the Soviet Ship Vulnerability Program (SSVP), a series of technology homework work unit plans were conducted. This program on effect of nose shape on penetration by a projectile was one of these technology homework programs conducted at NWC and under contract at the Denver Research Institute.

The work on this task was accomplished by the Denver Research institute under Contract No. N00123-69-C-1970. This work unit was funded by CNM through Naval Air Systems Command AirTask A-350-5321/008B/3F32-353-501.

This report has been reviewed for technical accuracy by M. H. Keith and is released at the working level for information only.

ABSTRACT

Target vulnerability analyses consider ballistic penetrators which
have various nose shapes. Nose shape often undergoes changes during
the target penetration process due to deformation. It is important
that the effects of nose shape upon ballistic perforation dynamics be
known and accounted for in vulnerability analyses. An experimental
firing program was conducted in which rigid penetrators having three
different nose shapes were fired against steel plate. Experimental
data generated concerned ballistic limit velocity, residual velocity,
and ricochet obliquity. Experimental data were compared with predictions
of analytic models. The prediction models were modified to reflect the
results of experiments.

THE EFFECT OF PROJECTILE NOSE SHAPE UPON
BALLISTIC LIMIT VELOCITY, RESIDUAL
VELOCITY, AND RICOCHET OBLIQUITY

Contract Number N00123-72-C-0267
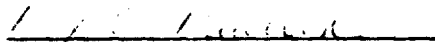
Prepared for

Weapons Development Department
Naval Weapons Center
China Lake, California

February 1973
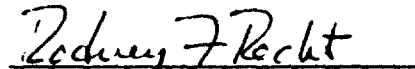
Denver Research Institute
of the
University of Denver

APPROVED BY: PREPARED BY:

Rex E. Paulsen, Head   Tom W. Ipson
Mechanical Sciences Division   Research Engineer

                                          Rodney F. Recht
                                          Senior Research Engineer

                                          William A. Schmeling
                                          Research Engineer

NOMENCLATURE

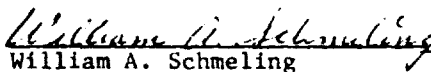a   Exponential coefficient, dimensionless

B   Coefficient in V_{50} equation; $= \tau \ln\left[\dfrac{(2Z_m)}{6\left(\dfrac{K\rho}{g}\right)^{1/2}}\right]$, ft/sec

BHN   Plate hardness, Brinell hardness number

b   Exponent in empirical V_{50} equation, dimensionless

C   Coefficient in empirical V_{50} equation, ft/sec

CA   Coefficient in $V50$ equation; $(0.0396/\left(\dfrac{K\rho}{g}\right)^{1/2}$; for steel plate $= 0.000305$), dimensionless

d   Projectile diameter, inch

e   Base for natural logarithms, dimensionless

E   Young's Modulus of plate material, lb/in^2

E_p Young's Modulus of projectile material, lb/in^2

E_e Maximum elastic energy in projectile, in-lb

f   Dynamic sliding coefficient of friction (0.01), dimensionless; Also used to denote "function of:

g   Gravitational constant (386), in/sec^2

h_{dc} Parameter, descriptive of false nose formed on projectile, dimensionless

K   Plate material bulk modulus, lb/in^2; also used in ricochet model as a constant of portionality, dimensionless

L   Effective length of projectile, inch

ℓn Natural logarithm, dimensionless

M_p Projectile weight, lb

M_s Weight of plate plug, lb

n   The fraction $(V_{50n} - V_{50nb})/(V_{50ns} - V_{50nb})$ at $\alpha = \alpha_c$, dimensionless; also used as empirical constant in ricochet model, dimensionless

R_c Projectile hardness, Rockwell C scale

T   Plate thickness, inch

V   Projectile impact velocity, ft/sec

V_h Ricochet velocity component parallel to plate surface, ft/sec

V_n Ricochet velocity component normal to plate surface, ft/sec

V_r Residual velocity, ft/sec

V_{50} Ballistic limit velocity, ft/sec

V_{50n} Ballistic limit velocity at normal incidence, ft/sec

$(V_{50n})_b$ V_{50n} for blunt rigid projectiles, ft/sec

$(V_{50n})_s$ V_{50n} for sharp rigid projectiles, ft/sec

W   Projectile weight (same as M_p), lb

W_1 Weight of equivalent projectile, lb

y   Deviation from $(V_{50n})_s$, ft/sec

z   Deviation from $(V_{50n})_b$, ft/sec

Z_m $Z_m = \dfrac{E}{\sigma}\left[\dfrac{1}{1 + \dfrac{2E}{\sigma}}\right]^{1/2}$, dimensionless

α Half angle of projectile conical nose (effective conical half angle of non-conical nose), deg

α_c Value of α which divides nose angles into sharper and blunter categories, deg

δ Total deflection of impact surface due to penetration and flexure, inch

Δ_c $(V_{50n})_s - (V_{50n})_b$ at $\alpha = \alpha_c$, ft/sec

θ Impact obliquity, measured with respect to plate normal, deg

θ_r Ricochet obliquity, measured with respect to plate normal, deg

ρ Specific weight of plate material, lb/in^3

ρ_p Specific weight of projectile material, lb/in^3

σ Static tensile strength of plate material, lb/in^2

σ_p Compressive ultimate strength of projectile material, lb/in^2

τ Static compressive shear strength of plate material, lb/in^2

CONTENTS

INTRODUCTION

There exists a need for a knowledge of the effects of nose shape upon the ballistic perforation characteristics of projectiles. Vulnerability analyses concerned with missile warheads, bombs, penetrating type projectiles, and projectiles which change nose shape during perforation due to crushing or fracture must consider the effects of nose shape upon ballistic limit velocities, residual velocity, and ricochet angles. Current perforation prediction models analytically define the role of nose shape in ballistic perforation. Data for correlating these analytical definitions is sparse. It was the objective of this research effort to experimentally examine the effects of nose shape upon ballistic perforation and to compare the data thus generated with predictions of the analytical model. Based upon these comparisons, modifications to the models would then be made to improve predictive capabilities where necessary.

A 300-round firing program was conducted in which rigid steel projectiles having three different nose shapes were fired at three thicknesses of steel plate. Obliquities of 0, 30, and 60 deg were investigated. The data generated concerned ballistic limit velocities, residual velocities, and ricochet angles.

Experimental results were compared with predictions of analytical models. Predictive methods for ballistic limit velocities were modified to account for unexpectedly dramatic effects of projectile hardness. These modified methods produce excellent correlations of ballistic limit velocity and residual velocity data. A model for prediction of ricochet obliquity was developed.

Reported herein is a description of the experimental procedure employed during the firing program, a presentation of the experimental results, and comparisons between predictions of analytical models and experimental data.

EXPERIMENTAL RESULTS AND COMPARISON
WITH MODEL PREDICTIONS

EXPERIMENTAL PROCEDURE

Firing Setup

Special 50-caliber steel projectiles were fired from a standard Mann Test Barrel having a 15-inch twist. The velocity was controlled by the amount and type of powder used. The projectiles were spin-stabilized by means of an integral gas seal and rotation band machined on the projectiles. Yaw cards were employed to monitor projectile stability at impact. Only data for stable (zero yaw) projectiles were recorded. Initial (impact) and residual (post perforation) velocity measurements were accomplished by systems of contact switches and chronographs.

Projectile Characteristics

Caliber 0.50 projectiles were machined from 4340 steel and heat-treated to a hardness of Rockwell C 50 to 55. The weight of all test projectiles was intended to be 410 grains. Due to miscalculations, the initial batch of projectiles produced were 445 grains. These were used in initial test series. All other test projectiles weighed 410 grains. Projectiles having three different nose shapes were used in the firing program--two conical-point and one blunt (flat) ended. The conical points were of 30 and 60 deg interior half angles (α). Figure 1 is a photograph of the three test projectiles.
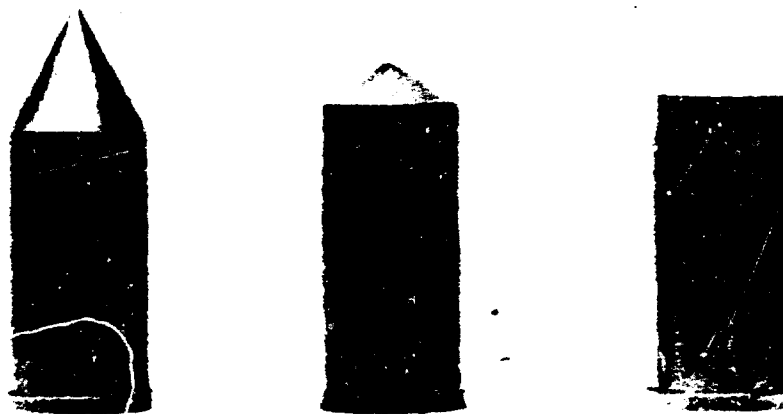

FIG. 1. Test Projectiles 0.50 Caliber, 410 Grains, 4340 Steel Heat-Treated to a Hardness of R_c 53; Conical Nose Half-Angle (Left to Right) 30, 60, and 90 Deg.

2

Target Plate Material

The plate material used in the test program was 4130 steel with a hardness of 220 and 260 BHN. Plate thicknesses used were 0.125, 0.250, and 0.375 inch. Eight-inch square plates were firmly clamped into the target assembly.

Ballistic Limit Velocity Determination

The ballistic limit velocity (V_{50})--defined in this study as the impact velocity for which there is a 0.5 probability that a projectile will have zero residual velocity--was determined by using the six-shot ballistic limit velocity procedure. Firing was conducted until three complete and three incomplete perforations were obtained within a velocity spread of 100 ft/sec or 10% of the ballistic limit velocity (whichever was lower). These six velocities were then averaged to obtain the ballistic limit velocity. A complete perforation was defined as occurring when the projectile completely passed through the plate (had some measure of residual velocity). This V_{50} corresponds very closely to the *Navy Criteria Ballistic Limit Velocity*. Figure 2 illustrates a typical set of V_{50} testing data. During the firing, if a complete perforation was obtained, the next test was conducted at a lower velocity; if an incomplete perforation was obtained, then the following test was fired at a higher velocity. This practice (within the limits of producing the desired velocity changes by means of small changes in propellent loads) insured staying within the zone of mixed results once it was found.

Ricochet Obliquity

Limited ricochet tests were fired with the three test projectiles against 0.250-inch-thick 4130 steel plate at 30 deg obliquity. The initial velocity was measured by the previously mentioned method. The angle of ricochet (defined in the same manner as obliquity; i.e., with respect to the plate normal) was determined from impacts upon wooden witness targets. The projectile would ricochet off the target plate into the wooden witness target, leaving an impact impression. From the geometry of the plate configuration and the wooden witness target, the ricochet angles were easily measured by noting the location of the impression made by the ricocheting projectile. The ricochet trajectory was essentially in the same plane as the obliquity angle.
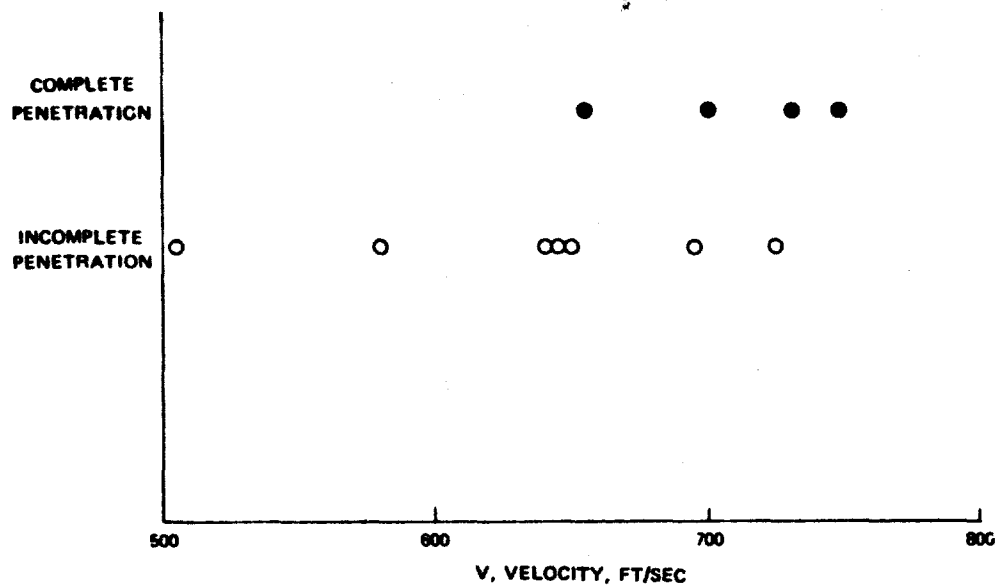
3

FIG. 2. Typical Ballistic Limit Velocity Data; 410-Grain, 4340 Steel Projectile (R_c 53), Conical Nose Half-Angle of 30 Deg; 0.125-Inch-Thick 4130 Steel (230 BHN) Plate, 0-Deg Obliquity.

EXPERIMENTAL RESULTS

Important ballistic perforation parameters which the projectile nose shape may influence are ballistic limit velocity, residual velocity, and angle of ricochet. The results of the experimental investigation of these parameters as functions of projectile nose shape are presented in the following.

Ballistic Limit Velocity

Ballistic limit velocities were determined for fourteen impact conditions involving various combinations of projectile nose shapes, plate thicknesses, and obliquities. Table 1 lists the ballistic limit velocity results of these tests. The projectile nose shape is described in terms of nose half-angle, (α). Recall that this angle is the interior half angle of the conical point. A small angle corresponds to a sharp point, a larger angle to a blunter conical nose. An (α) of 90 deg is the flat-faced projectile.

4

TABLE 1. Experimental Ballistic Limit Velocities Determined for
Rigid Steel Projectiles and 4130 Steel (230 BHN) Plate.

T, inches	θ, deg	W, grains	α, deg	V_{50}, ft/sec	$V_{50n}/\cos\theta$
0.125	0	410	30	692	-
0.125	0	410	60	717	-
0.125	0	410	90	651	-
0.125	30	410	30	782	(798)
0.125	30	410	60	787	(827)
0.125	30	410	90	-	(750)
0.125	60	410	30	1410	(1385)
0.125	60	410	60	-	-
0.125	60	410	90	-	-
0.250	0	445	30	1290	(1 -
0.250	0	450	60	901	-
0.250	0	410	90	893	-
0.250	30	410	30	1422	(1490)
0.250	30	450	60	1232	(1040)
0.250	30	410	90	-	-
0.250	60	410	30	-	-
0.250	60	445	60	2218	(1800)
0.250	60	410	90	-	-
0.375	0	410	30	1536	-
0.375	0	410	60	1193	-
0.375	0	410	90	1297	-

Figure 3 presents normal (0-deg obliquity) ballistic limit velocity
data as a function of projectile nose half-angle for three thicknesses
(T) of 4130 steel plate--0.125, 0.250, and 0.375 inch. Seven of the
nine data points represent 410-grain projectiles. The two data points
for the tests with 30- and 60-deg α against 0.250-inch plate were
obtained with 445-grain projectiles. The dashed lines indicate the
trend of the data. The trend line for the 0.250-inch thickness is
drawn above the two data points for the 445-grain projectiles. As
indicated by the data on Fig. 3, against the thin (0.125-inch) plate,
the effect of nose shape is very slight; the ballistic limit velocities
determined for nose half-angles of 30, 60, and 90 deg show a maximum
difference of 66 ft/sec. Against the thicker plates (0.250 and
0.375 inch), the data indicates a higher ballistic limit velocity for
a nose half-angle of 30 deg as compared to that obtained for half angles
of 60 and 90 deg. Little difference is noted between the data obtained
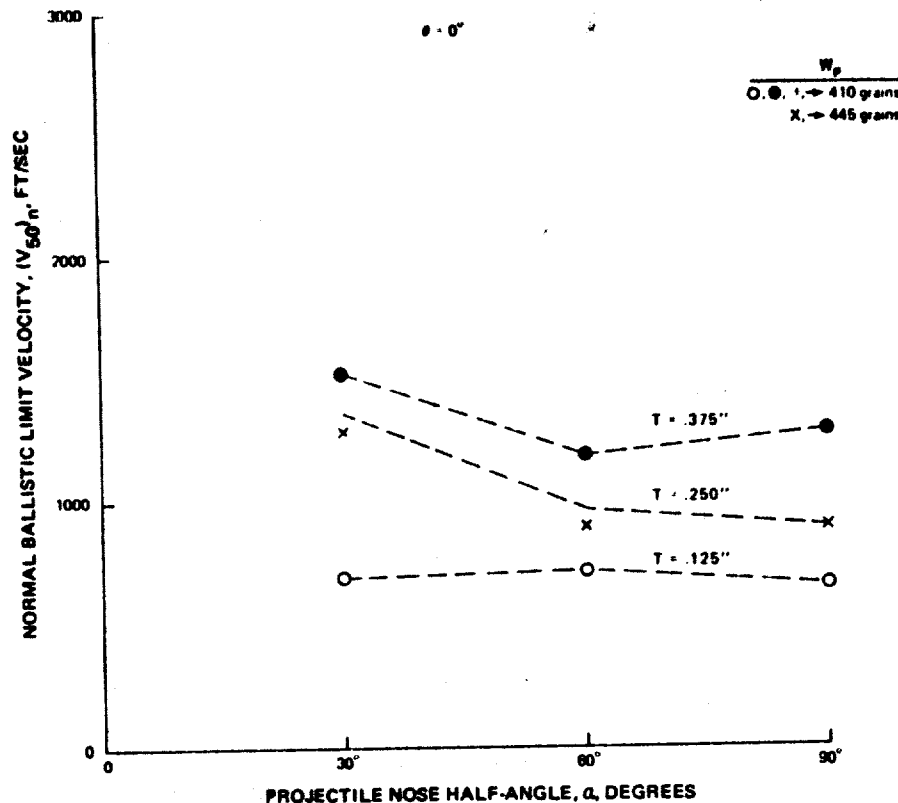for projectiles characterized by 60- and 90-deg nose half-angles.

FIG. 3. Experimental Results; Ballistic Limit Velocity as a Function of Projectile, Nose Half-Angles (30, 60, and 90 Deg) Against 4130 Steel (230 BHN) Plate of 0.125-, 0.250-, and 0.375-Inch Thickness, 0 Deg Obliquity. Dashed Lines Show Data Trend.

Figure 4 compares ballistic limit velocity/nose-shape data obtained against 0.125-inch thick steel plate at obliquity with data obtained at normal incidence. This figure contains data points for the $\alpha = 30$ deg projectile fired at 30 and 60 deg obliquity and for the $\alpha = 60$ deg projectile fired at 30 deg obliquity. The dashed lines labeled 30 and 60 deg obliquity were obtained by multiplying the 0-deg obliquity data trend line by the secant of the obliquity angle. The oblique data points correlate very well with these lines. This illustrates that for projectiles with various nose shapes, the ballistic limit velocity at obliquity can be closely approximated by multiplying the normal ballistic limit velocity by the secant of the obliquity angle. This procedure also works well for ogival armor penetrating projectiles and blunt fragments (Ref. 1).
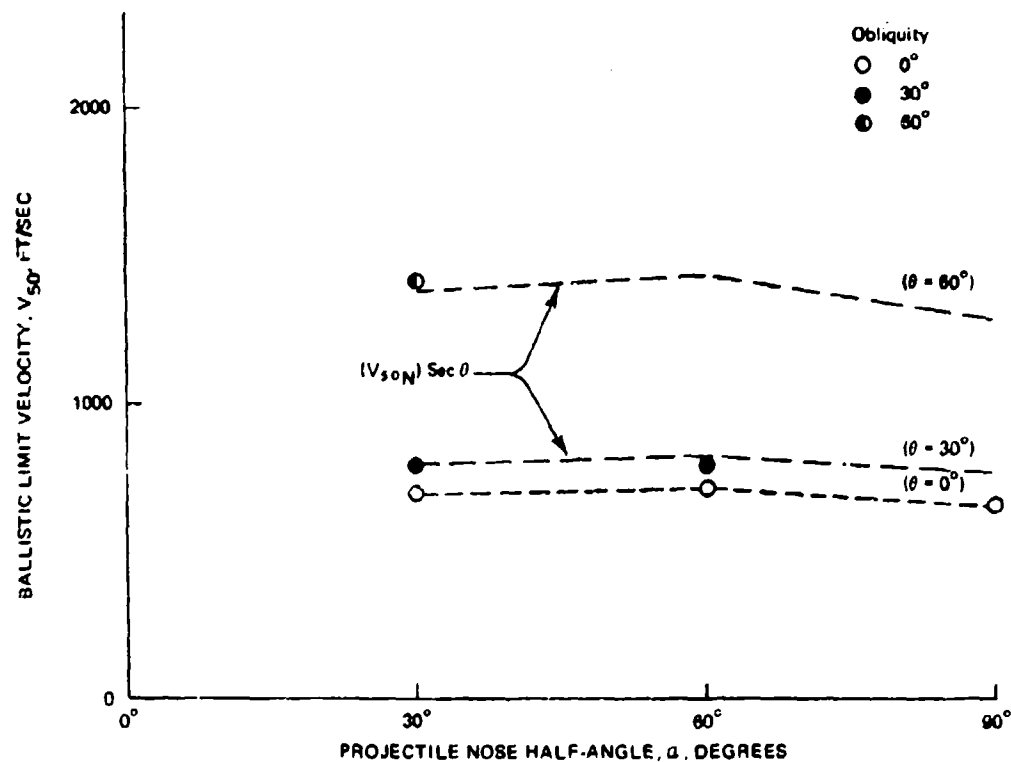
6

FIG. 4. Experimental Results at Obliquity; Ballistic Limit Velocity as a Function of Projectile Nose Half-Angle; Comparison of Oblique Data With Normal Data; 0.125-Inch 4130 Steel (230 BHN) Plate, 0-, 30-, and 60-Deg Obliquities.

The ballistic limit velocity values experimentally determined for the α = 90 deg test projectiles were much lower than were anticipated. Previous research efforts (Ref. 2) with blunt elongated fragments had shown analytical equations (Ref. 3) for blunt-nosed projectiles to be very accurate in predicting ballistic limit velocities. The ballistic limit velocity data obtained for the α = 90 deg projectiles were well below those predicted by these equations. It became obvious from inspection of impacts and perforations made in the target plates that projectile rigidity had to be playing a major role in the differences being produced. The rigid (R_c 53), blunt (α = 90 deg) projectiles used in this research effort produced clean, square-bottomed impressions in the target plates at sublimit velocities. At velocities above the ballistic limit, plate perforations had the appearance of machined-like holes. Softer (R_c = 30) non-rigid fragments, for which the predictive equations were derived, deform upon impact and expend much more energy in projectile and plate deformation. To prove that the difference in experimental ballistic limit velocities as compared with predictions

was attributable entirely to projectile rigidity, a test series using
$\alpha = 90$ deg, 410-grain projectiles having a hardness of R_C 30 was con-
ducted against 0.250-inch steel plate at 0 deg obliquity. This test
series produced a ballistic limit velocity of 1,698 ft/sec. The ballis-
tic limit velocity determined for the R_C 53 fragment under exactly the
same conditions was 893 ft/sec. Figure 5 illustrates the physical
difference in the plate and projectile deformations associated with
impacts and perforations by the two types of projectiles. The projec-
tiles shown in the photograph are ones recovered after impacting at
velocities just below the ballistic limit velocity. Note the amount of
deformation experienced by the soft (R_C 30) projectile. The rigid
(R_C 53) projectiles exhibited no deformation during any of the tests
conducted during this research effort. Compare the plate deformations
for both the incomplete and the complete perforations. The rigid pro-
jectile, by not deforming, maintains a concentrated shear stress
gradient for promoting plugging. The non-rigid projectile, as it
deforms, becomes a much less efficient penetrator and thereby must have
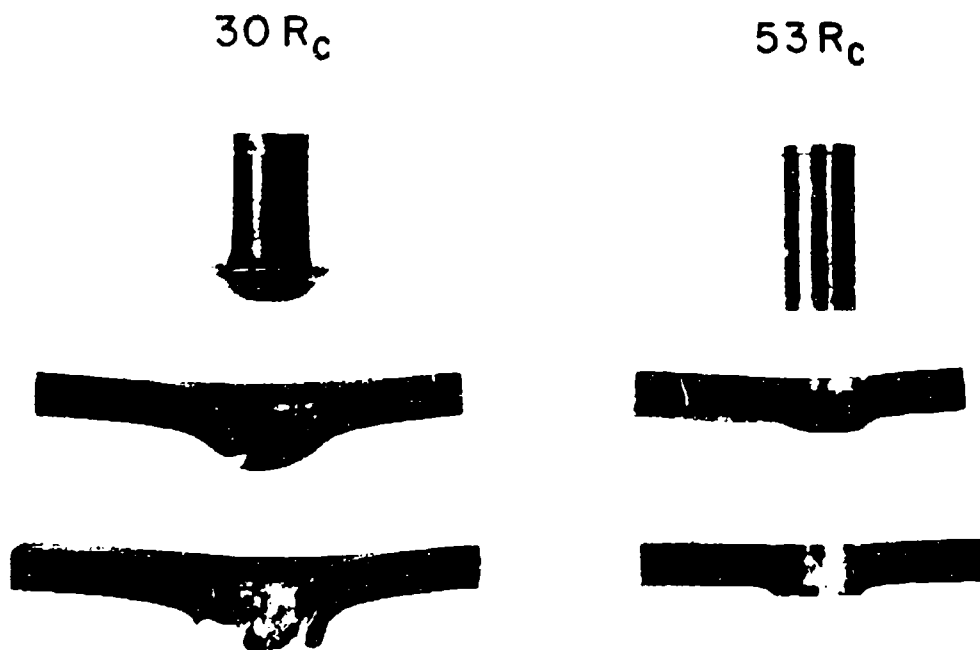a much higher impact velocity to achieve perforation.

$30\,R_C$ $53\,R_C$

FIG. 5. Effect of Penetrator Harness on Projectile and Plate Deformation at Velocities
Just Below and Above the Ballistic Limit Velocity.

The stated objective of this project was to study the effects of nose shape upon the ballistic perforation behavior of rigid projectiles. The startling V_{50} results obtained for rigid flat-nosed projectiles necessitated modifications to the theoretically developed equations for predicting ballistic limit velocities for rigid projectiles with blunt nose shapes. Prior to this experimental investigation, most data available pertaining to blunt nose shapes concerned projectiles of a nominal hardness of 30 R_c. Consequently, efforts to account for nose shape relied upon data for rigid armor-piercing projectiles at the sharp end of the nose-shape spectrum and data for blunt, non-rigid fragments at the other end of the spectrum. Modifications of the analytical predictive methods for rigid penetrators of various nose shapes are discussed in the next section, *Comparisons of Experimental Data and Predictions of Analytical Model* (p. 15).

Residual Velocity

Measurements of residual velocity were made for four of the fourteen test conditions investigated. Figures are included herein which present projectile residual velocity data as a function of impact velocity. Also plotted on these figures are the prediction curves of the residual velocity equation (Ref. 1 and 3) for penetrating-type projectiles. This equation (which applies to standard armor-piercing projectiles) has the form:

$$V_r = \sqrt{V^2 - V_{50}^2} \tag{1}$$

Equation 1 applies to projectiles which perforate plates by displacing plate material radially rather than by driving a plug from the plate. For the latter perforation mode (blunt projectiles), the applicable form of the DRI residual velocity equation includes terms which account for the momentum of the material ejected from the plate. For the blunt projectiles (high values of the nose half-angle, α), the DRI residual velocity equation is:

$$V_r = \sqrt{\frac{V^2 - V_{50}^2}{1 + \dfrac{M_s}{M_p}}} \tag{2}$$

where

M_s is weight of the plate plug material, lb

M_p is weight of the projectile, lb.

For flat-ended (α = 90 deg) projectiles, M_s is very closely estimated by the weight of the plate material which lies in the path of the perforating projectile, or:

$$M_s = \frac{\rho \pi d^2 T}{4 \cos \theta} \qquad (3)$$

Note that Eq. 2 reduced to Eq. 1 when the M_s term is zero. As the nose half-angle, α, becomes larger (a projectile becomes blunter), there should be a transition from the penetration mode to the plugging mode when perforating relatively thin plates. The specific objective of the residual velocity experiments was to examine the relationship between M_s and nose shape with respect to accurate residual velocity prediction. Residual velocity data are presented with the predictions of Eq. 1 (M_s assumed to be zero) for comparison purposes.

Figure 6 displays residual velocity data obtained with the sharp pointed 410-grain, α = 30 deg projectile against 0.125-inch thick 4130 steel plate at 0 deg obliquity. Also plotted on this figure is the residual velocity prediction curve of Eq. 1. The value used for the V_{50} value is that determined experimentally for this impact configuration. Figure 6 shows very good agreement between the experimental residual velocity data and the prediction curve of Eq. 1. Correlation with Eq. 1 indicates that there is very little influence of plate material (M_s) upon the residual velocity for this impact condition.
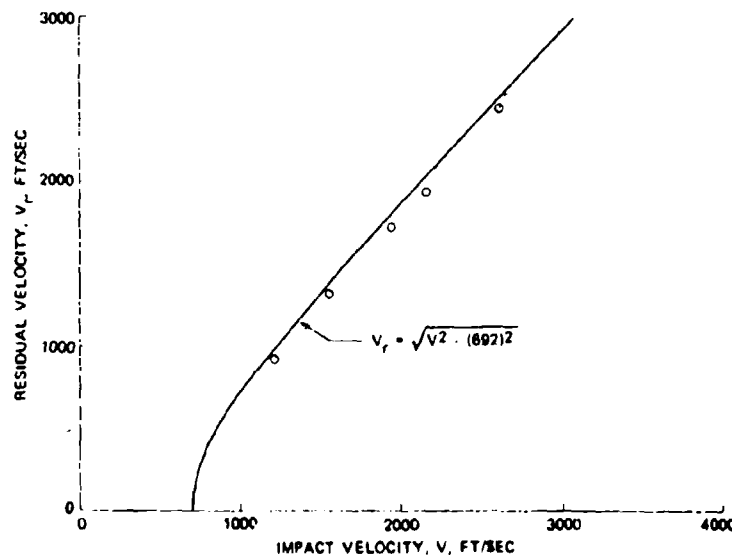

FIG. 6. Residual Velocity as a Function of Impact Velocity; 0.125-Inch 4130 Steel Plate (230 BHN); 410-Grain. a = 30-Deg Rigid Projectile (53 R_c), 0-Deg Obliquity.

10

Figure 7 presents residual velocity data for the same projectile
but against thicker plate (0.250 inch). These data show good agreement
with the prediction curve of Eq. 1 at the lower values of residual veloc-
ity. The data point at an impact velocity just less than 3,000 ft/sec
is well below the prediction curve. This may indicate that at the
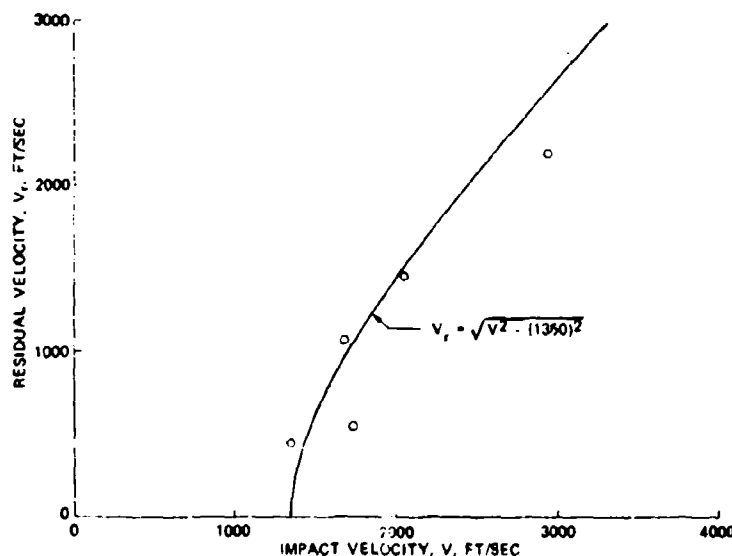higher velocities even a relatively sharp nose does plug out some plate
material.

FIG. 7. Residual Velocity as a Function of Impact Velocity;
0.250-Inch 4130 Steel Plate (230 BHN); 410-Grain, a =
30-Deg Rigid Projectile (53 R_c), 0-Deg Obliquity.

Residual velocity data for the blunter (α = 60 deg) projectile is
shown in Fig. 8. The target plate is 0.125-inch 4130 steel at 0 deg
obliquity. These data also show very good correlation with prediction
of Eq. 1. Plate plugs were recovered from the projectile trap. Figure 9
shows a photograph of a typical plate plug recovered from residual
velocity test series with the (α = 60 deg) projectile and 0.125-inch and
0.250-inch target plates. On Fig. 8, the prediction of Eq. 2 (which
considers the plate plug) is also shown (dashed curve). The ratio of
the plate plug mass to the projectile mass (M_s/M_p) is small (0.113) with
this thin plate, and Eq. 2 predicts only slightly lower residual velocity
than Eq. 1. The effect of the plate plug mass upon residual velocity is
well illustrated by the data obtained with the α = 60 deg) projectile
and the 0.250-inch plate. Figure 10 presents these data together with
the residual velocity predictions of both Eq. 1 and 2. As may be seen,
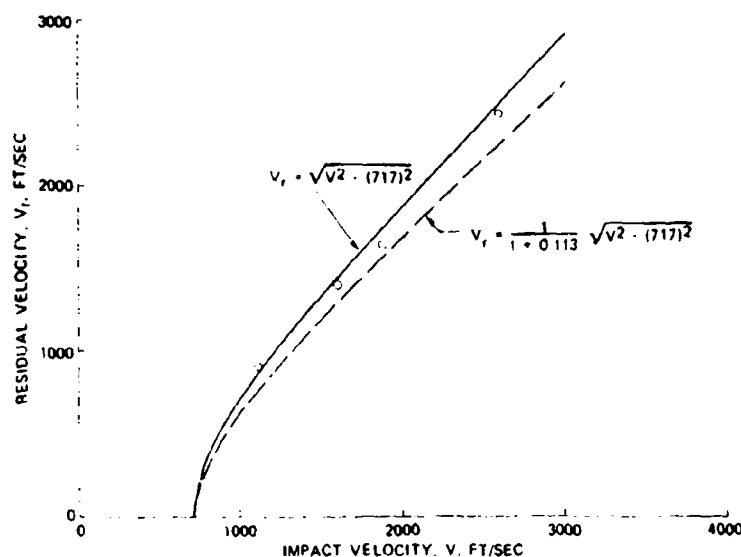the experimental data agrees with the prediction of Eq. 2, as it should.

11

$$V_r = \sqrt{V^2 - (717)^2}$$

$$V_r = \frac{1}{1 + 0.113} \sqrt{V^2 - (717)^2}$$

FIG. 8. Residual Velocity as a Function of Impact Velocity; 0.125-Inch 4130 Steel Plate (230 BHN); 410-Grain, $a = 60$-Deg Rigid Projectile (53 R_c), 0-Deg Obliquity.

This experimental investigation of the effect of nose shape upon perforation mode and associated effect upon residual velocity has shown that, in the range of plate thickness studied, the ($a = 30$ deg) projectile tended to perforate without producing a plate plug and that the ($a = 60$ deg) projectile acted in the same manner as a flat-ended projectile and perforated by the plate plugging process. Allowances for nose shape when predicting residual velocity are discussed in detail in the next section, *Comparisons of Experimental Data and Predictions of Analytical Model*.

Ricochet Obliquity

Angles of ricochet associated with an impact obliquity of 30 deg were measured in test firings involving 0.250-inch 4130 steel target plate and each of the three test projectiles ($a = 30$, 60, and 90 deg). Figure 11 presents the ricochet obliquity (θ_r) data obtained as a function of impact velocity. Ricochet obliquity is measured with respect to the plate normal as is impact obliquity. The data for each of the three projectiles is differentiated by means of the symbols employed. Note that the ricochet obliquity is large (the ricochet direction is nearly parallel to the surface of the target plate) at low impact velocities. At higher velocities (as the ballistic limit velocities are approached), the ricochet angle decreases. This occurs as the result of plate deformation (flexure and surface penetration); the projectile is deflected upward while escaping the impact impression.
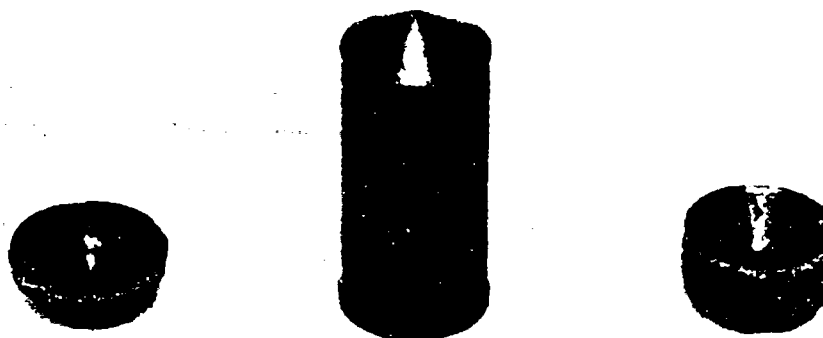
12

FIG. 9. Conical Nosed Rigid Projectile (a = 60 Deg) and Typical Plate Plugs from 0.125-Inch (Left) and 0.250-Inch (Right) 4130 Steel (230 BHN) Plate; 0-Deg Obliquity.
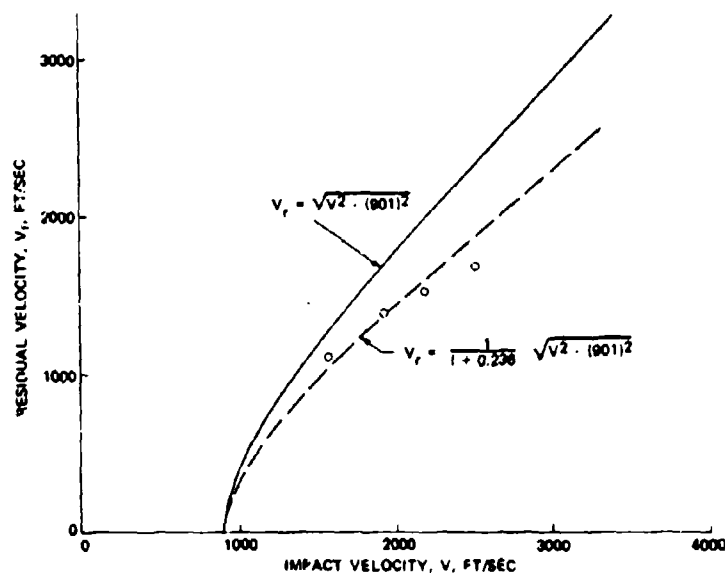

FIG. 10. Residual Velocity as a Function of Impact Velocity; 0.250-Inch 4130 Steel Plate (230 BHN); 410-Grain, a = 60-Deg Rigid Projectile (53 R_c), 0-Deg Obliquity.
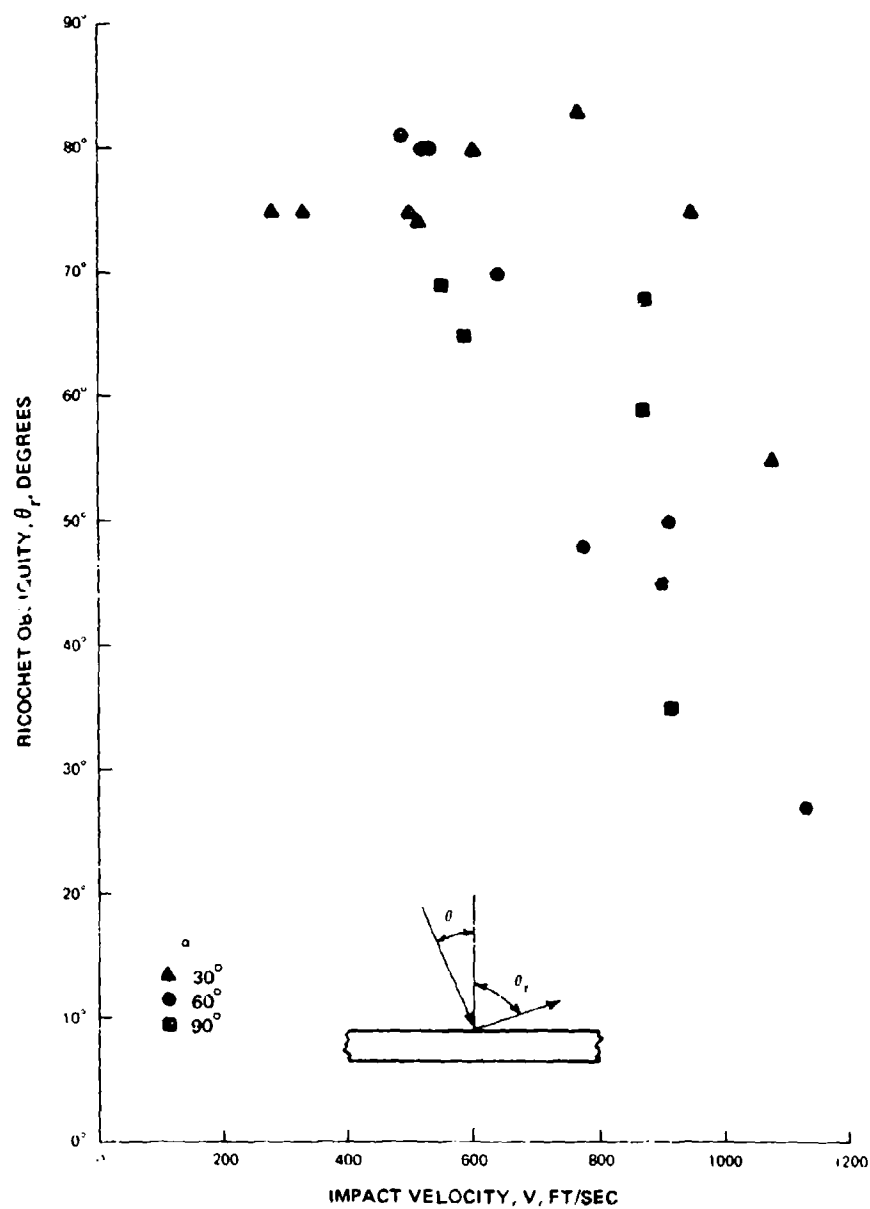
13

FIG. 11. Ricochet Obliquity Angle Data as a Function of Impact Velocity; Rigid 4340 Steel (53 R_c) Projectiles of 30-, 60-, and 90-Deg Nose Half-Angles (α) Ricocheting From 0.250-Inch 4130 Steel Plate (230 BHN); 30-Deg Obliquity.

14

Figure 12 is a plot of the ricochet angle data as a function of the ratio of impact velocity to the individual ballistic limit velocity of the particular projectile involved. Plotting in this manner tends to group the data and better illustrates the manner in which the ricochet angle changes with impact velocity. Data in Fig. 11 and 12 do not display any distinctive differences in ricochet angle due to differences in nose shape. For rigid projectiles, it would appear from the results of this study that the angle of ricochet can be considered as being independent of nose shape. Although this study was limited to one impact obliquity and one plate thickness, if the influence of nose shape upon ricochet angle was significant, this effect should have been evident in these experimental results.

COMPARISONS OF EXPERIMENTAL DATA AND PREDICTIONS OF ANALYTICAL MODEL

In 1970, the Surface Target Vulnerability Program, JTCG/ME (through the Naval Weapons Center, China Lake), supported a research program at the University of Denver Research Institute (DRI). Its objective was to develop a suitable multiple plate perforation model which could be used to predict the penetration of large-caliber projectiles, guided missile warheads, and bombs into ship structures (Ref. 3). This model incorporates methods for considering various projectile parameters such as nose shape. This present experimental investigation was performed to obtain data which could be used to improve prediction capabilities of the ship penetration model (SPM) as related to nose shape. The prediction models for ballistic limit velocity, residual velocity, and ricochet obliquity were modified. These models are discussed.

Ballistic Limit Velocity

Predictions of the ship penetration model were inaccurate when compared with the experimental ballistic limit velocity data generated in this program. This inaccuracy is attributable to the dramatic influence that projectile deformation exerts upon ballistic limit velocity. In the original penetration model for rigid penetrators, the submodel which considered variations in nose shape was based upon considerations of data for armor-piercing projectiles (representative of sharp penetrators) and fragment-simulating projectiles (representative of flat-ended or blunt penetrators). Armor-piercing projectiles have a hardness of 63 R_c. Since there was an absence of data for rigid, flat-ended projectiles, fragment simulator data was used. It was felt that the hardness of these projectiles (29-31 R_c) was sufficient to represent rigid projectiles for the small values of T/d (plate thickness/penetrator diameter) typical during ship penetration. The results of this study illustrate the strong influence which penetrator deformation exerts upon the ballistic limit velocity of steel plates (see previous discussion related to Fig. 5). It has been shown that rigid projectiles, to be
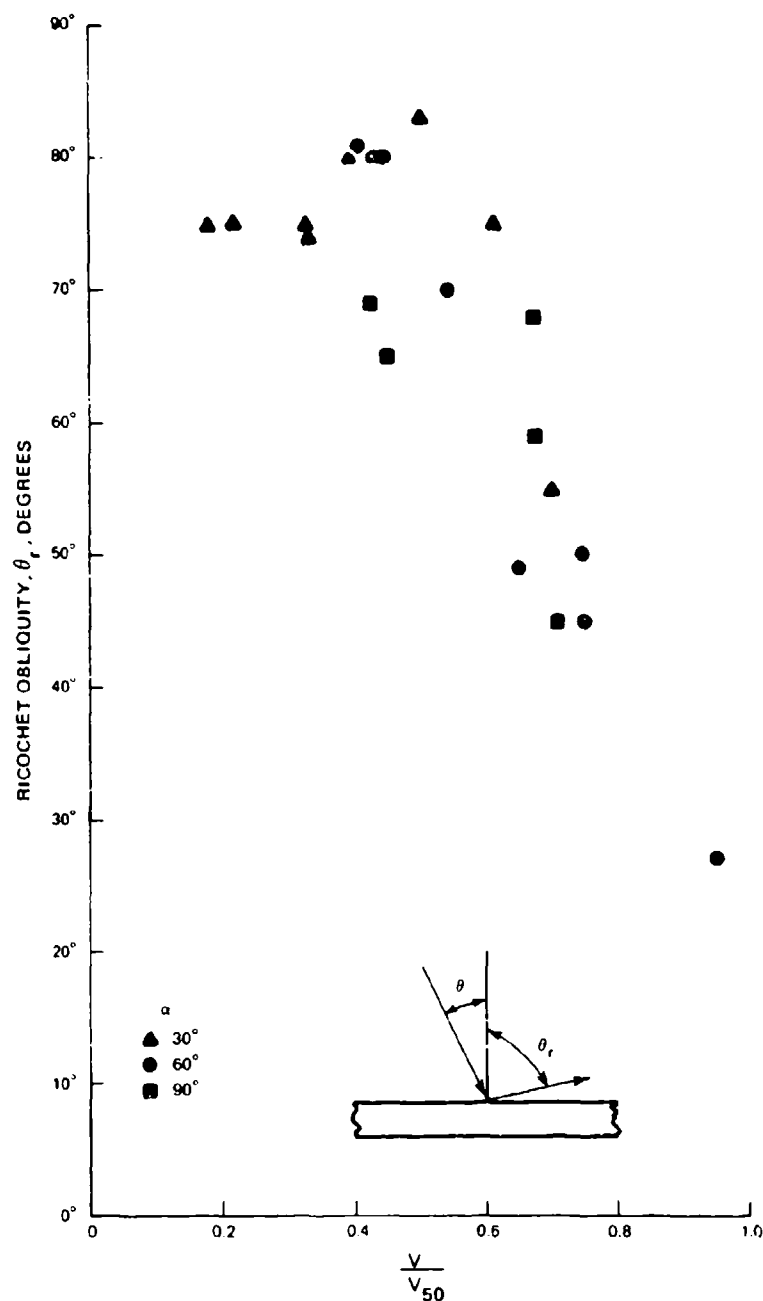
15

FIG. 12. Ricochet Obliquity Angle Data as a Function of Normalized Impact Velocity; Rigid 4130 Steel (53 R_c) Projectiles of 30-, 60-, and 90-Deg Nose Half-Angles (a) Ricocheting From 0.250-Inch 4130 Steel Plate (230 BHN); 30-Deg Obliquity.

considered as such, must truly remain rigid (exhibit almost no impact deformation) and that there can be a dramatic increase in ballistic limit velocity as projectile hardness decreases.

Based upon the results of the tests with the flat-ended (α = 90 deg) projectiles, the ship penetration model was modified. In Fig. 13, the nine circular data points are the same as presented in Fig. 3. The three triangular points do not represent firing data, but are interpretations of experimental data curves for monobloc projectiles (Ref. 4). They apply to 0.50-caliber, 410-grain rigid projectiles having standard armor-piercing ogives (equivalent to a conical nose having a nose half-angle of 14.5 deg; Ref. 3). The three dashed curves shown on Fig. 13 are the predictions of the ship penetration model for "sharp" rigid projectiles. This equation (*DRI Sharp Projectile Equation*) is:

$$T/d = \frac{2.5(CA)(W/d^3)}{\sin\alpha + f\cos\alpha}\left\{(V_{50n})_s - \frac{B}{\sin\alpha}\ \ell n\left[1 + \frac{(V_{50n})_s\ \sin\alpha}{B}\right]\right\} \tag{4}$$
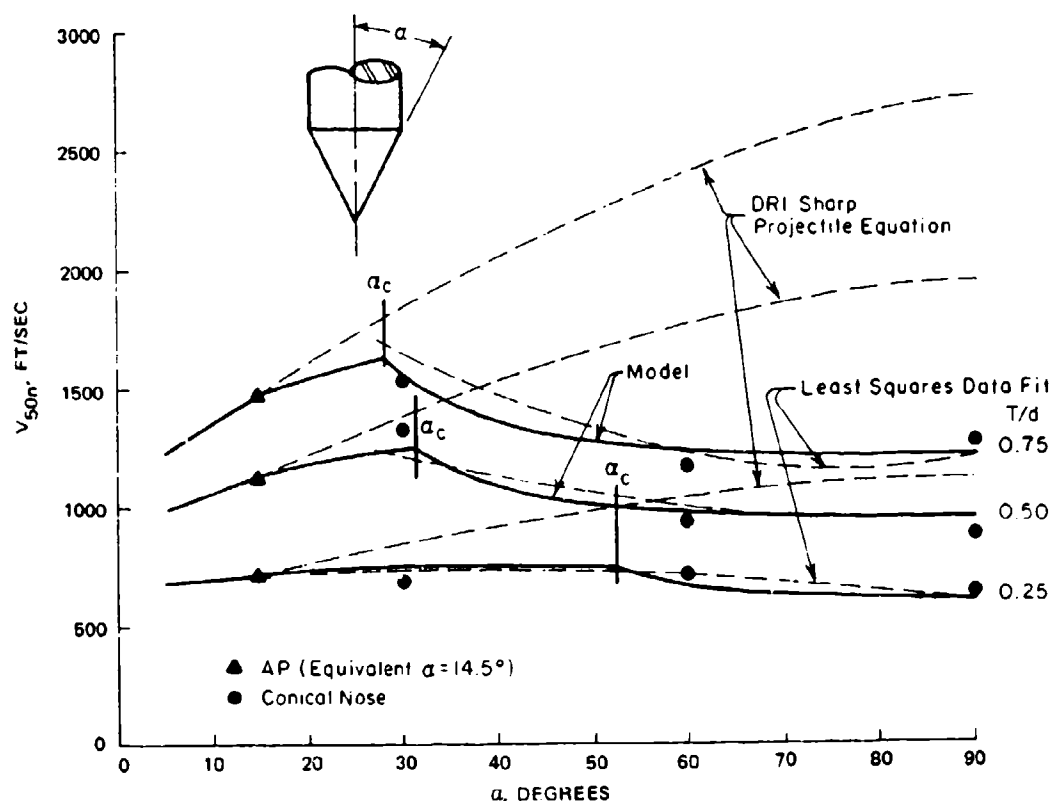

FIG. 13. Correlation of Ballistic Limit Velocity Data as a Function of Projectile Nose Shape; Rigid Steel Projectiles (53 R_c); Steel Plate (230 BHN).

As α increases, the projectile nose geometry changes from "sharp" to "blunt." Obviously (from comparing the prediction of Eq. 4 with the data points), the transition from "sharp" to "blunt" starts somewhere between α = 15 deg and α = 30 deg, and is essentially complete before α = 60 deg (i.e., the experimental results at α = 60 deg are essentially the same as at α = 90 deg). The three values shown in Fig. 13 for α_c (the critical nose half-angle) were determined as outlined in the ship penetration final report (Ref. 3) (and in the following discussion), and are estimates of the boundary between "sharpness" and "bluntness" (i.e., the appearance of plugging during perforation). The three solid curves in Fig. 13 represent the model developed to predict $(V_{50})_n$ as a function of nose shape as characterized by α. Following is a brief description of the model. (The model will be presented in detail subsequently.)

1. For α < 15 deg, Eq. 4 for sharp penetrators is used to predict $(V_{50})_n$.

2. For 15 deg < α < α_c, a computed value of the parameter y (a linear function of α - 15 deg) is subtracted from the solution of Eq. 4 to predict $(V_{50})_n$.

3. For α_c < α < 90 deg, a computed value of the parameter z (an exponential function of α - α_c) is added to the (V_{50n}) value for flat-ended projectiles to predict (V_{50n}).

4. For α = 90 deg an equation of the following form is used to predict (V_{50n}):

$$(V_{50n}) = C(W/d^3)^a(T/d)^b \tag{5}$$

where a, b, and C are constants which depend upon plate properties and projectile characteristics.

Note that at the lowest T/d value (Fig. 13), there is very little change in $(V_{50})_n$ with nose shape. Data for lower T/d values are hard to obtain due to the low velocities involved; since it was demonstrated that $(V_{50})_n$ is insensitive to changes in α at T/d = 0.25, it was not necessary to perform such low velocity experiments.

The data plotted on Fig. 13 pertain to T/d values of 0.25, 0.50 and 0.75. Rigid projectiles which are characterized by low α values tend to penetrate by pushing material aside so as to produce a hole and are referred to as "sharp." Rigid projectiles which are characterized by high α values tend to push material ahead so as to produce a plate plug during perforation and are referred to as "blunt." Armor-piercing projectiles are "sharp" and flat-ended projectiles are "blunt;" projectiles having α values in between retain attributes of "sharp" and "blunt" projectiles to varying degrees.

Equation 4 pertains to projectiles which can be classified as "sharp." As was stated, Eq. 4 was used to generate the three curves (dashed above $\alpha = 15$ deg) which rise from left to right on Fig. 13. The AP (sharp projectile data, triangular symbols) fall on these curves, but the data at $\alpha = 30$ deg fall below the three curves indicating that the associated projectiles already exhibit some attributes of "bluntness." Obviously, the projectiles possessing nose half-angles of 60 deg are behaving essentially as "blunt" projectiles. (Plate plugs produced by $\alpha = 60$-deg and $\alpha = 90$-deg projectiles are quite similar in appearance; see Fig. 9.) The three dashed curves associated with the circular data points are least squares fits to the data for the three T/d values.

A prediction model would compute $(V_{50})_n$ for "sharp" projectiles using Eq. 4, and would compute $(V_{50})_n$ values for blunt penetrators using an equation applicable to $\alpha = 90$ deg. It would accomplish a transition between the "sharp" and "blunt" predictions for α values between 15 and 90 degrees. The following approach was used to develop the model for rigid projectiles which provides the prediction represented by the solid curves in Fig. 13.

Sharp Projectiles. For $\alpha < 15$ deg, Eq. 4 is used.

Flat-Ended Projectiles. For $\alpha = 90$ deg and $T/d < 1$, the following form correlates data pertaining to flat-ended rigid projectiles:

$$(V_{50})_n = C \, (W/d^3)^a (T/d)^b \tag{5}$$

where

W = weight of projectile, lb

d = diameter of projectile, in.

T = plate thickness, in.

C, a, and b are constants which vary with plate material and projectile characteristics.

Above $T/d = 1$, the projectile is forced to penetrate to considerable depth before driving a plug from the plate and the $(V_{50})_n$ is higher than that predicted by Eq. 5. For $L/d = 2$ and 4130 steel plate heat-treated to 230 BHN the following equation applies to the above conditions for $\alpha = 90$ deg:

$$(V_{50})_n = 930 \left(\frac{T/d}{W/d^3}\right)^{0.61} = 1475 \, (T/d)^{0.61} \tag{6}$$

Determination of the Critical Nose Half-Angle, α_c. A critical value of the nose half-angle (i.e., α_c) which serves to separate "sharpness" from "bluntness" can be determined by considering that during penetration a flat-ended penetrator picks up a false nose (a physical fact when penetrating thick plates) made up of plate material which redefines the nose shape. Then, as outlined in Ref. ?, the projectile can be represented by a sharp projectile with a nose half-angle, α_c, a weight, W_1, equal to the weight of the original projectile plus the false nose, and a velocity V_1 which is $(W/W_1)(V_{50n})$--thereby conserving momentum: (V_{50n}) is the limit velocity of the original projectile. The plate thickness in the representation is taken to be T_1 which is less than T due to the transfer of plate material to the projectile. Given this sharp projectile and thinner plate representation, Eq. 4 can be used with Eq. 6 to establish a relationship between α_c and T/d for given values of CA, B, and f. That is, since $(V_{50})_n$ for the representative projectile must be equal to that of the actual flat-ended projectile, Eq. 6 can be substituted into Eq. 4 for $(V_{50})_n$ for wherein T is replaced by T_1, CA is replaced by $(W_1/W)CA$, $(V_{50})_n$ is replaced by $(W/W_1)(V_{50})_n$, and α is replaced by α_c.

$$\frac{W_1}{W} = 1 + \pi\rho \ \frac{(T/d + T_1/d)}{4 \ (W/d^3)} \ . \tag{7}$$

where ρ is specific weight of plate material, lb/in^3.

If h_{dc} is defined as being:

$$h_{dc} = \frac{1}{2 \ \tan \alpha_c} \tag{8}$$

and if $T/d \geq h_{dc}$, then

$$T_1/d = T/d - \frac{h_{dc}}{3} \tag{9}$$

otherwise

$$T_1/d = T/d - (h_{dc}/3) + \frac{(h_{dc} - T/d)^3}{3 \ h_{dc}^3} \tag{10}$$

Making the previously mentioned substitutions into Eq. 4, the following equation results:

$$T_1/d = \frac{2.5(CA)(W_1/W)(W/d^3)}{(\sin \alpha_c + f \cos \alpha_c)} \left\{ (V_{50})_n (W/W_1) \right.$$

$$\left. - \frac{B}{\sin \alpha_c} \ell n \left[1 + \left(\frac{(V_{50})_n \sin \alpha_c}{(W_1/W)B} \right) \right] \right\} \tag{11}$$

Substitution of Eq. 7, 9, and 10 into Eq. 11 results in the aforementioned relationship between α_c and T/d which can be resolved by iteration, both with respect to the variables and the conditions pertaining to Eq. 9 and 10. Curves of α_c versus T/d for various values of B (or plate hardness, BHN, which is directly related to B) can be constructed so that α_c values can be determined rapidly. The α_c values applying to the three T/d values used in this experimental program are shown on Fig. 13. Figure 14 shows the α_c versus T/d relationship computed for the 230 BHN, homogeneous steel plate used.
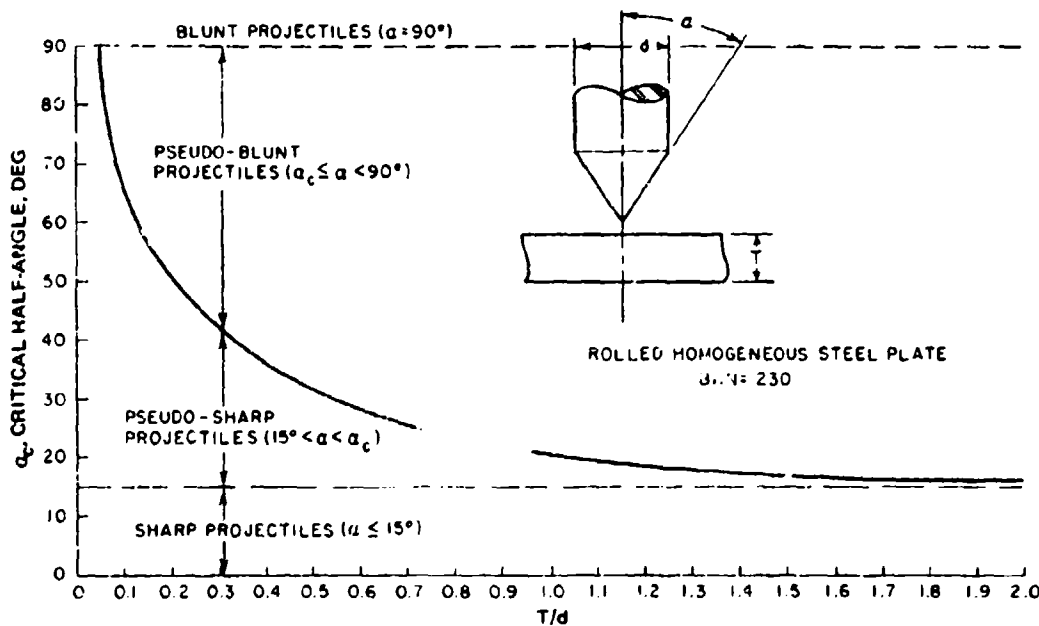
FIG. 14. Computed Critical Nose Half-Angle (a) as a Function of T/d for Rolled Homogeneous Steel Plate (230 BHN).

The Transition from "Sharp" to "Blunt." The change from "sharp" to "blunt" as α increases, would not be expected to take place suddenly at some value, α_c; it would be expected to be transitional. Further, the above procedure for computing α_c merely provides a reasonable estimate of the boundary between "sharpness" and "bluntness." Figure 13 suggests that $(V_{50})_n$ values will begin to deviate from the "sharp" curve generated by Eq. 4 as α becomes larger than 15 deg. As values become larger than α_c, plugging should develop rapidly. Consequently, the transition suggested by Fig. 13 is proposed as being representative of observations and expected behavior. Figure 15 illustrates the transitional model which utilizes the ballistic limit velocity predictions for sharp $(V_{50n})_s$ and blunt $(V_{50n})_b$ projectiles.
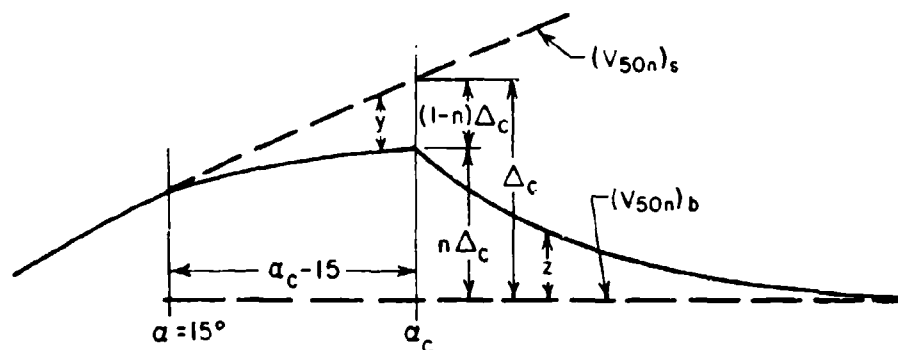
FIG. 15. Model for Predicting Transitional Values of Ballistic Limit Velocity.

For values which lie between 15 deg and α_c, the value for $(V_{50})_n$ computed by Eq. 4 is diminished by an amount (y) to obtain a transitional value for $(V_{50})_n$. For values exceeding α_c, the $(V_{50})_n$ value for a flat-ended projectile is increased by z to obtain a transitional value of $(V_{50})_n$. The parameter Δ_c represents the difference between the $(V_{50})_n$ value computed by Eq. 4 at α = α_c and the $(V_{50})_n$ value computed for a flat-ended projectile (Eq. 5); thus $(n\Delta_c)$ represents the value of z at α = α_c and $(1 - n)$ Δ_c represents the value of y at α = α_c (where n has some value between 0 and 1). Obviously, n is 1 at α = 15 deg and 0 at α = 90 deg. If y is assumed to be linear with α, then

$$y = (1 - n) \Delta_c \left(\frac{\alpha - 15 \text{ deg}}{\alpha_c - 15 \text{ deg}} \right) \qquad (12)$$

22

If z is assumed to decrease exponentially with α, then

$$z = n \Delta_c \, e^{-a(\alpha - \alpha_c)} \tag{13}$$

Letting $a = 0.1$ is appropriate with respect to the data plotted on Fig. 13.

The dashed curves representing least squares fits of Fig. 13 (their values at $\alpha = \alpha_c$) can be used to determine a relationship for n as a function of α_c. These three values are plotted along with two other known values on Fig. 16. The curve on Fig. 16 represents the following equation:

$$n = 0.000148(\alpha_c - 15 \text{ deg})^2 - 0.0244(\alpha_c - 15 \text{ deg}) + 1 \tag{14}$$
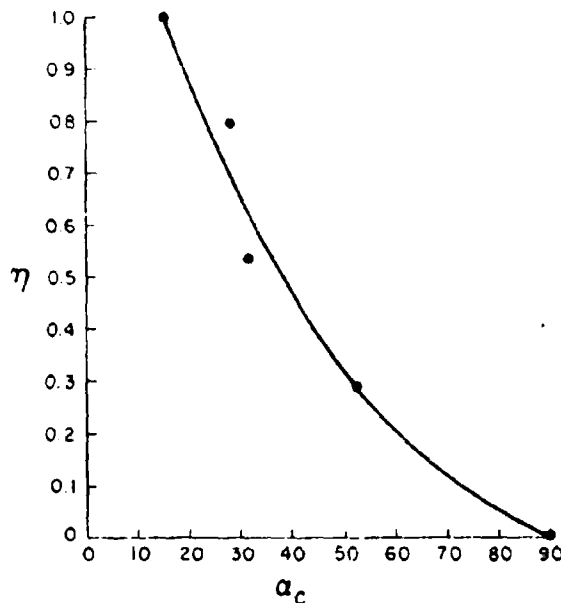
FIG. 16. Relationship Between Parameter (η) and Critical Nose Half-Angle (α_c).

For "Semi-Sharp" Projectiles, $15 \text{ Deg} < \alpha \leq \alpha_c$. As indicated above, the $(V_{50})_n$ for semi-sharp projectiles is computed as follows:

$$(V_{50})_n = (V_{50n})_s - (1 - n) \Delta_c \left(\frac{\alpha - 15 \text{ deg}}{\alpha_c - 15 \text{ deg}} \right) \tag{15}$$

where $(V_{50n})_s$ is $(V_{50})_n$ as computed using Eq. 4 and Δ_c is the difference between $(V_{50n})_s$ as computed by Eq. 4 (at $\alpha = \alpha_c$) less $(V_{50n})_b$ as computed by Eq. 6 ($\alpha = 90$ deg).

23

For "Semi-Blunt" Projectiles, $\alpha_c < \alpha < 90$ Deg. As indicated above, the $(V_{50})_n$ for semi-blunt projectiles is computed as follows:

$$(V_{50})_n = (V_{50n})_b + n \Lambda_c e^{-0.1 (\alpha - \alpha_c)} \tag{16}$$

where $(V_{50n})_b$ is the $(V_{50})_n$ as computed using Eq. 6.

Application and Limitations of the $(V_{50})_n$ Prediction Model. The solid curves on Fig. 13 were generated using the prediction model outlined above. In its present form, the model applies to rigid projectiles which are characterized by projectile length-to-diameter ratio equal to 2. It is limited to T/d values less than 1.0 and to steel plates characterized by BHN equal to 230. It can be used for projectiles having other (L/d) values and plates with different characteristics simply by replacing Eq. 6 by the appropriate equation for flat-ended projectiles and using this new equation with Eq. 4 to compute α_c values as described above. Also the limitation of T/d can be lifted if Eq. 6 is replaced by an equation valid for T/d values above 1.0.

Residual Velocity

In the previous section, *Experimental Results*, residual velocity data generated during the experimental firing program were presented in graphical form, (Fig. 6, 7, 8, and 10) and compared with the prediction of Eq. 1 using the experimental value of $(V_{50})_n$. Equations 1 and 2 predict residual velocity; the applicability of one or the other is dependent upon the comparison between α and α_c. For "sharp" penetrators ($\alpha \leq \alpha_c$), Eq. 1 applies. For "blunt" penetrators ($\alpha > \alpha_c$) Eq. 2 applies. Figures 17, 18, 19, and 20 compare residual velocity data with the prediction of Eq. 1 or 2, whichever applies. The $(V_{50})_n$ values used in solution of these equations are those predicted by the previously discussed model and shown on Fig. 13.

Figure 17 presents residual velocity data for the $\alpha = 30$-deg projectile against 0.125-inch thick 4130 steel plate at 0 deg obliquity. The critical nose half-angle (α_c) predicted for this impact condition is equal to 53 deg (see Fig. 13). Since (α) is less than (α_c), Eq. 1 applies to the residual velocity prediction. The projectile is assumed to be behaving as a "semi-sharp" penetrator and perforating the plate without formation of a plate plug. Figure 17 shows excellent agreement between the experimental data and the curve predicted by Eq. 1.
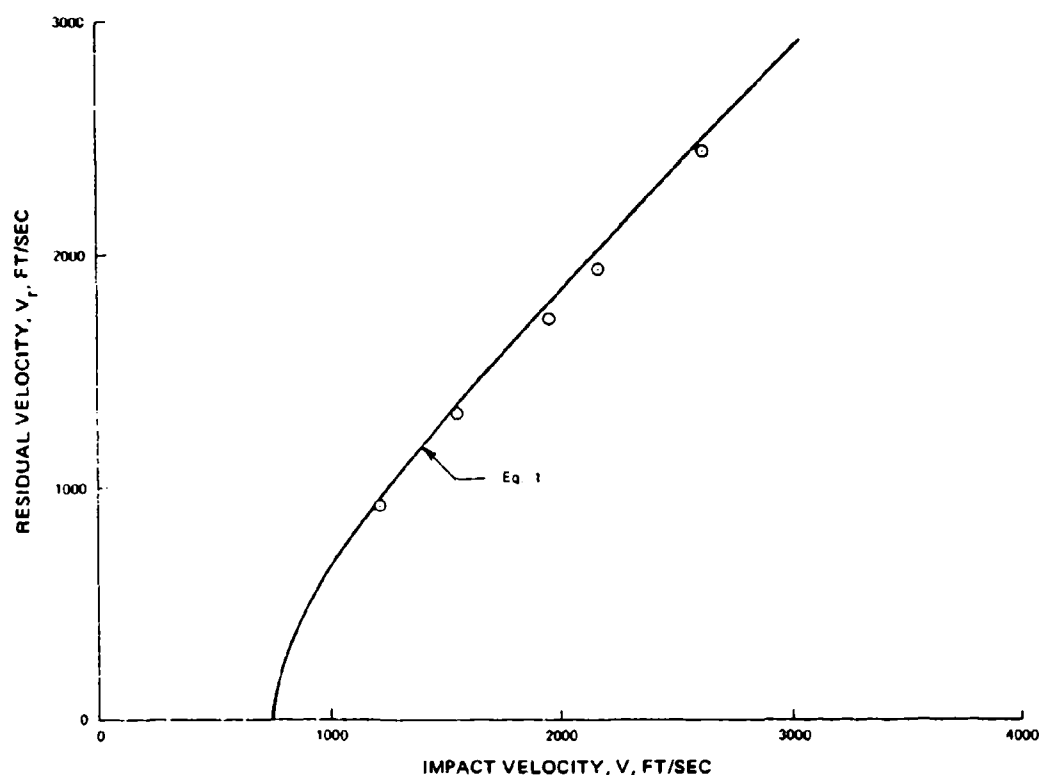
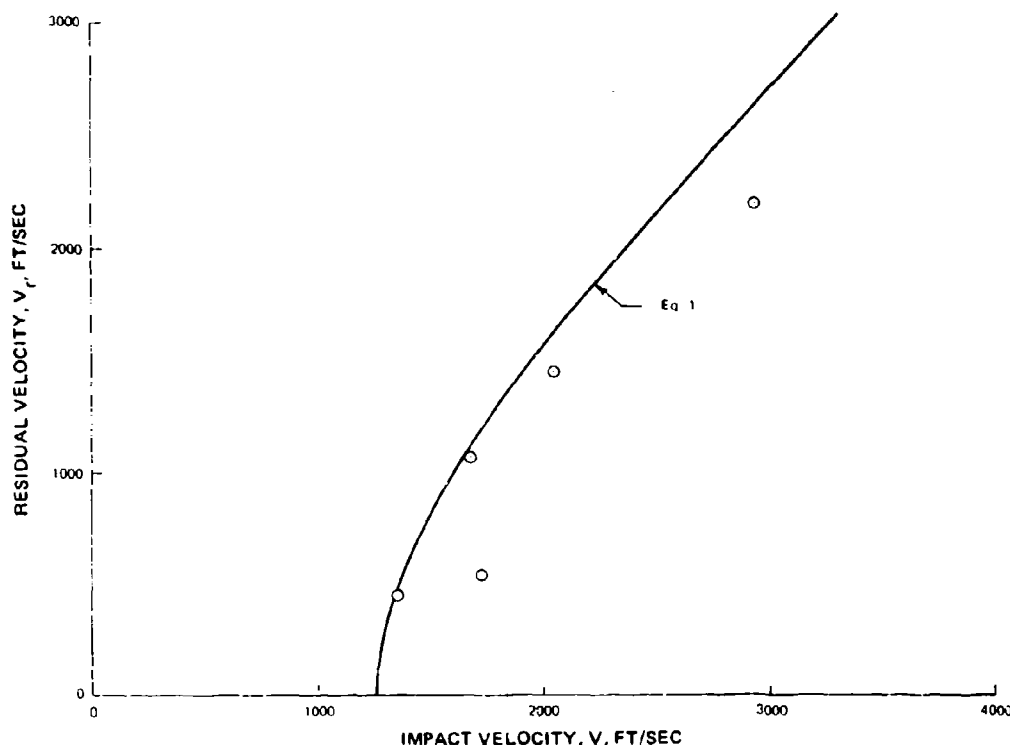FIG. 17. Correlation Between Residual Velocity Data and
Prediction of Eq. 1; 0.125-Inch-Thick 4130 Steel (230 BHN)
Plate; 410-Grain, a = 30-Deg Rigid Projectile.

Figure 18 presents the residual velocity data for the (α = 30 deg)
projectile perforating 0.250-inch-thick 4130 steel plate at 0 deg
obliquity; α_c for this condition is equal to 33 deg. Since α is again
less than α_c, Eq. 1 applies to the residual velocity prediction. As
seen on the figure, the higher velocity test data lie below the predic-
tion curve. These data points suggest that the plate may be plugging
and the momentum of the plate plug detracting from the residual velocity
of the projectile. However, the two lower velocity data points (the
data point at an impact velocity of 1,725 ft/sec should be ignored since
it appears to be an anomaly) correlate well with the prediction curve.
The fact that the predicted critical nose half-angle (33 deg) is so
close to the actual projectile nose half-angle (30 deg) suggests that
the projectile may be borderline between "sharp" and "blunt" behavior
and is performing as a sharp penetrator at the lower perforation
velocities, but is plugging the test plate at the higher velocities.

25

FIG. 18. Correlation Between Residual Velocity Data and
Prediction of Eq. 1; 0.250-Inch-Thick 4130 Steel (230 BHN)
Plate; 410-Grain, a = 30-Deg Rigid Projectile.

Figure 19 compares data with Eq. 2; in this case the critical nose
half-angle (53 deg) is less than the nose half-angle of the projectile
(60 deg). The plate is 0.125-inch-thick 4130 steel. The data plot
slightly above the prediction curve of Eq. 2, showing very good agree-
ment with the prediction curve.

Figure 20 again compares data with the prediction curve of Eq. 2.
For this test condition (0.250-inch-thick 4130 steel plate, α = 60 deg),
the predicted critical nose half-angle (33 deg) is well below the pro-
jectile nose half-angle. There is no doubt that this projectile is
behaving as a "blunt" penetrator as illustrated by the correlation
between the Eq. 2 prediction and the data. The prediction of Eq. 1 for
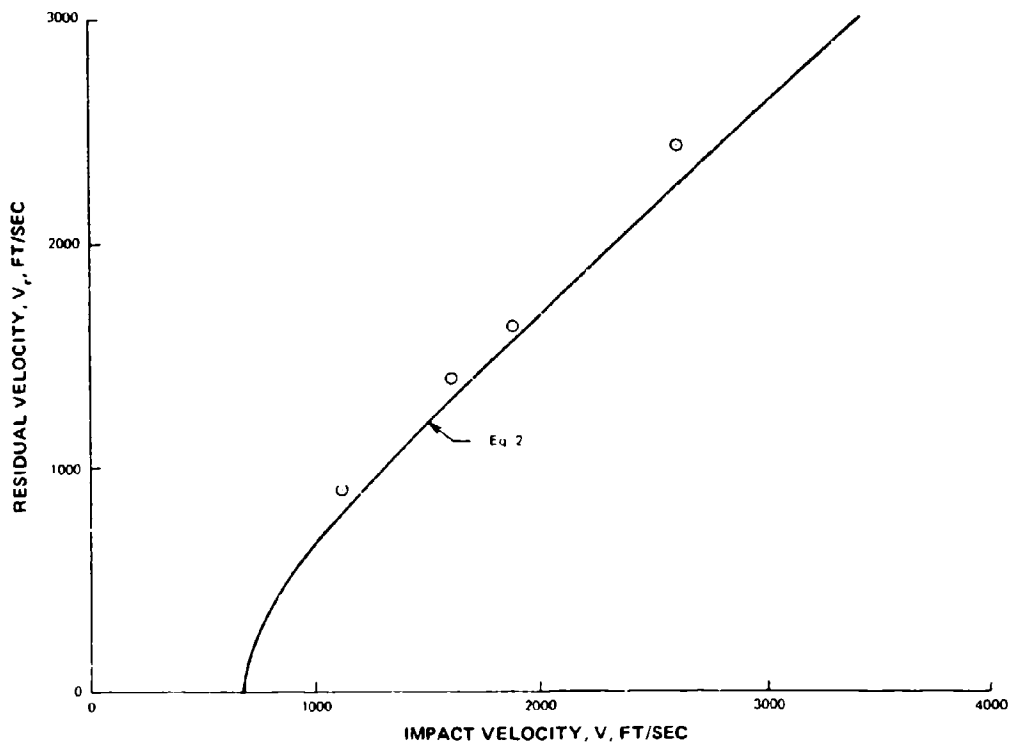these data would be 20% higher than the Eq. 2 curve shown in Fig. 20.

26
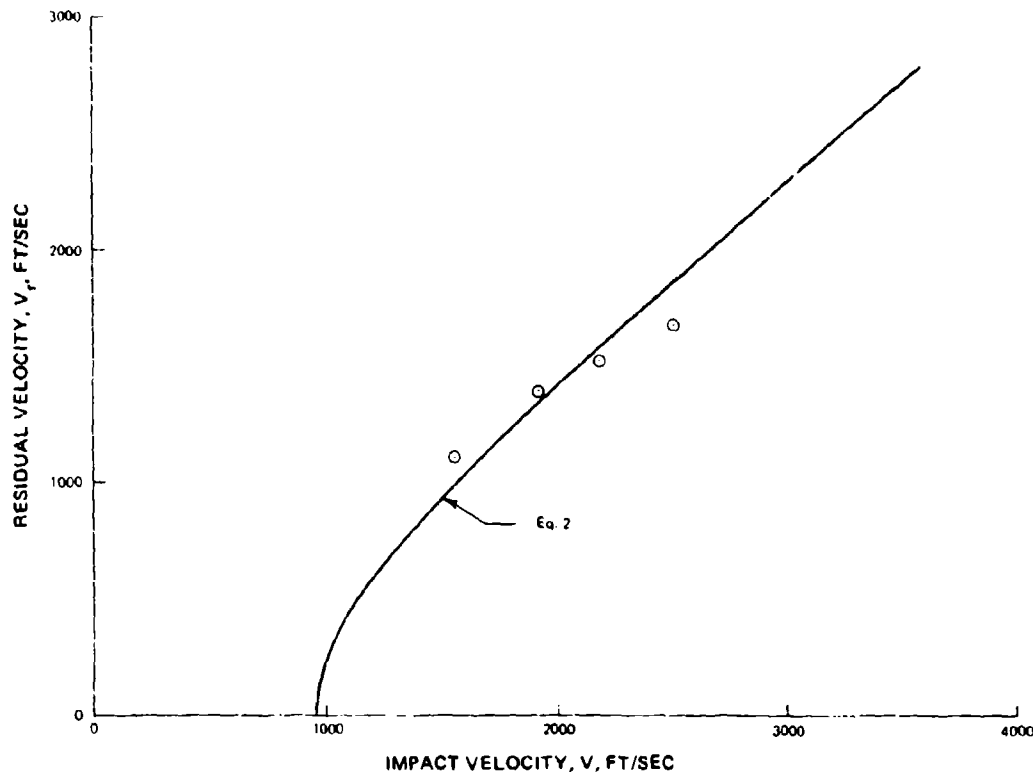
FIG. 19. Correlation Between Residual Velocity Data and
Prediction of Eq. 2; 0.125-Inch-Thick 4130 Steel (230 BHN)
Plate; 410-Grain, a = 60-Deg Rigid Projectile.

Ricochet Obliquity

The ricochet model incorporated within the Ship Penetration Model
(Ref. 3) provided an average value for the ricochet obliquity angle
(θ_r). The ricochet obliquity data are represented in Fig. 21. As dis-
cussed previously, the effect of projectile nose shape upon ricochet
angle as depicted by these data does not appear to be systematic,
deviations appearing to be chargeable to experimental scatter. For the
test condition pertaining to the data in Fig. 21, the ship penetration
model ricochet obliquity model predicts a ricochet obliquity of 66 deg,
independent of impact velocity. This predicted value depicts a good
average of experimental results, but does not define the observable
trend of the data wherein the ricochet obliquity appears to approach
the impact obliquity as the impact velocity approaches the ballistic
limit velocity.

FIG. 20. Correlation Between Residual Velocity Data and
Prediction of Eq. 2; 0.250-Inch-Thick 4130 Steel (230 BHN)
Plate; 410-Grain, a = 60-Deg Rigid Projectile.

The following ricochet model was developed for rigid projectiles
and steel plate based upon experimental observations of this and pre-
vious work (Ref. 5), and the physics of the ricochet problem. This
model incorporates means for including the effects of penetrator defor-
mation--not a consideration herein.

As long as the impacted surface remains undeformed and rigid,
ricochet dynamics are relatively easy to predict. The maximum elastic
energy which can be stored within a penetrator is equal to

$$E_e = \frac{1}{2} \frac{M_p}{\rho_p} \frac{\sigma_p^2}{E_p} \quad \text{(in-lb)} \tag{17}$$

28
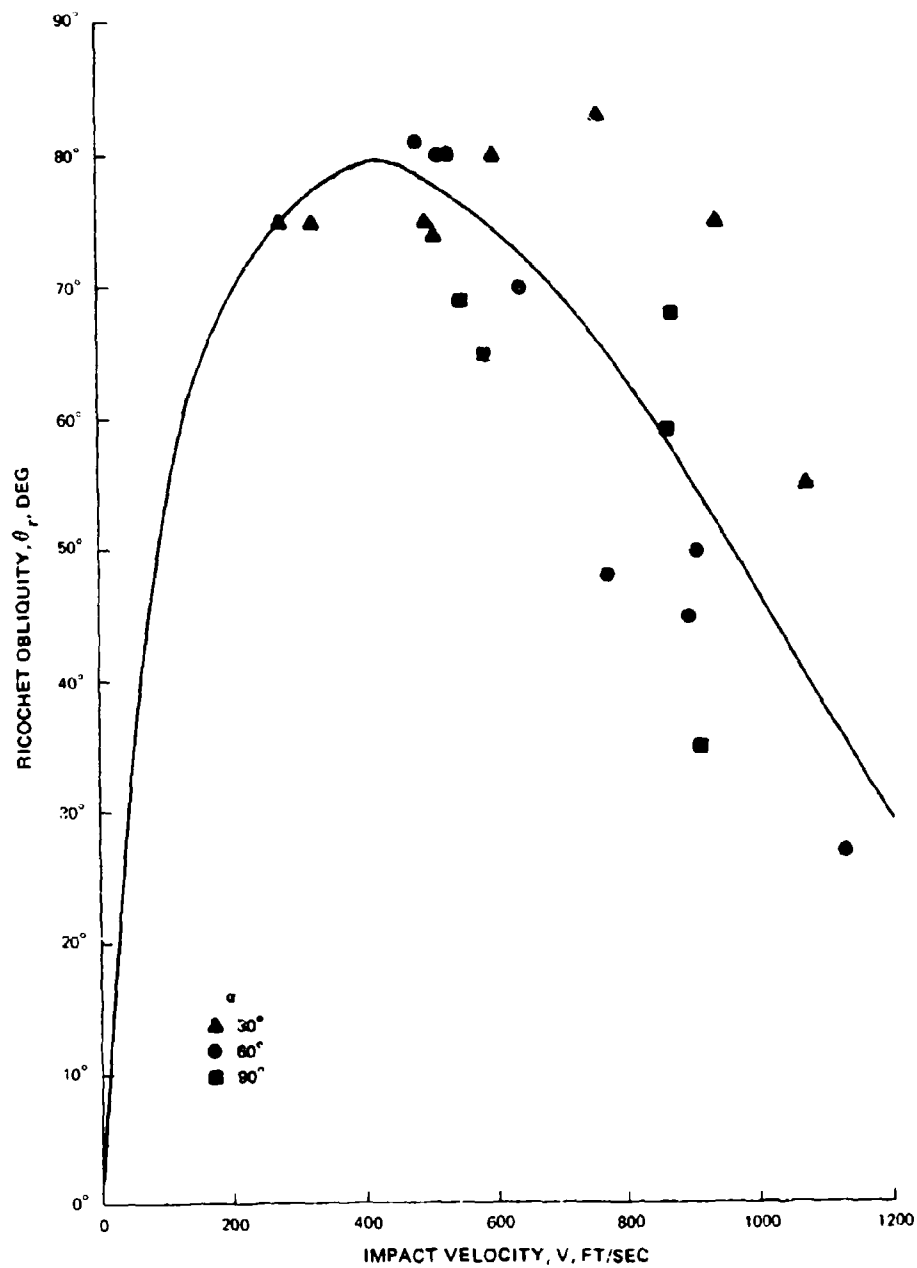
FIG. 21. Correlation Between Ricochet Obliquity Data and Eq. 25; 30-Deg Obliquity.

where

σ_p = specific weight of penetrator material, lb/in^3

σ_p = compressive ultimate strength of penetrator material, psi

E_p = Young's modulus of penetrator material, psi.

In such a ricochet situation the velocity component, V_h, parallel to the surface changes very little. The normal component, V_n, is defeated, elastic response of the penetrator being responsible for the normal component of the rebound velocity. Using this model, the two components of the ricochet velocity become

$$V_h = V \sin \theta \qquad \text{(ft/sec)} \qquad (18)$$

$$V_n = \frac{\sigma_p}{12} \sqrt{\frac{g}{\rho_p E_p}} \qquad \text{(ft/sec)} \qquad (19)$$

where

θ = impact obliquity, deg

g = acceleration of gravity, 386 in/sec^2

The tangent of the minimum (corresponding to maximum elastic energy) ricochet obliquity angle, θ_r, is then

$$\tan \theta_r = V_h/V_n = \frac{12 \sqrt{\rho_p E_p/g} \; V \sin \theta}{\sigma_p} \qquad (20)$$

According to this equation, a steel penetrator characterized by σ_p = 150,000 psi which impacts a rigid surface at an obliquity of 45 deg, and at 200, 500, and 1,000 ft/sec, will exhibit corresponding minimum ricochet obliquities (measured with respect to the plate normal) of 59, 77, and 83 deg. The softer the penetrator the more rapidly θ_r approaches 90 deg. Since the entire projectile will not be stressed to the ultimate stress, rebound will be less and θ_r values will be higher. The right side of Eq. 20 can be multiplied by a proportionality factor, J, to account for this, and an appropriate value can be determined from experiments.

Surface deformation will act to decrease ricochet obliquities by presenting a ramp to the parallel (with respect to the plate surface) motion, which will reduce the parallel component of ricochet velocity and increase the normal component. Surfaces are deformed in two ways, by surface penetration and by plate flexure. Letting δ be the total deflection due to penetration and flexure, dimensional analysis leads to the following functional relationship for a non-deforming penetrator:

30

$$\delta/d = f\left(T/d,\ \frac{M_p}{d^3}\ \frac{V^2 \cos^2 \theta}{g\sigma}\right) \tag{21}$$

The total normalized deflection, δ/d, will be the sum of the deflections due to penetration and flexure. Studies of the response of waveguide to ballistic impact have shown that the permanent flexural deflection is linear with respect to velocity below the ballistic limit velocity (Ref. 6). Further, this flexural deflection appears to be inversely proportional to the square root of the normalized thickness, T/d. Cratering (penetration) studies have shown that crater volume is approximately proportional to the impact energy; thus, deflection due to penetration is approximately proportional to the cube root of the kinetic energy. Measurements of flexure and penetration near the ballistic limit at normal incidence during these experiments (at $T/d = 0.5$) indicated that the flexural component was over twice as large. Penetration by a deforming penetrator will be related to its deformed diameter, D. These considerations lead to the following equation for deflection:

$$\frac{\delta/d}{K} = \left\{ \left[\frac{(M_p/d^3)(12V)^2 \cos^2 \theta}{(D/d)^3} \frac{}{g\sigma} \right]^{1/3} + 0.29 \left[\frac{(M_p/d^3)(12V)^2 \cos^2 \theta}{(T/d)} \frac{}{g\sigma} \right]^{1/2} \right\} \tag{22}$$

where K is an empirical constant of proportionality placed on the left side of the equation for convenience.

If Eq. 20 (modified by the proportionality constant, J, mentioned previously) defines the ricochet obliquity angle for a penetrator impacting a rigid plate, the following equation would be expected to define the ricochet obliquity for a penetrator impacting a non-rigid plate:

$$\tan \theta_r = \frac{12\ J\sqrt{\rho_p E_p/g}\ \ V \sin \theta}{\sigma_p} \left[1 + f\ \left(\frac{\delta/d}{K} \right) \right] \tag{23}$$

Using the data presented on Fig. 11 to plot $f[(\delta/d)/K]$ versus $(\delta/d)/K$ Eq. 23 was found to take the following form (which applies where $(\delta/d)/K > n/K$):

$$\tan \theta_r = \left[\frac{12\ J\sqrt{\rho_p E_p/g}\ \ V \sin \theta}{\sigma_p} \right] \exp\left[-m\left(\frac{\delta/d}{K} - \frac{n}{K} \right) \right] \tag{24}$$

where m and n are empirical constants. When $(\delta/d)/K \le n/K$ the exponential term is replaced by 1.0.

For the data plotted on Fig. 11 the following values of parameters apply:

$$M_p = 0.0586 \text{ lb}; \quad d = 0.5 \text{ in.};$$

$$T = 0.25 \text{ in.}; \quad \theta = 30 \text{ deg};$$

$$\rho_p = 0.283 \text{ lb/in}^3; \quad S = 115,000 \text{ psi};$$

$$\sigma_p = 270,000 \text{ psi}; \quad E_p = 30 \times 10^6 \text{ psi}; \quad D/d \approx 1$$

Using these values, Eq. 24 and 22 become

$$\tan \theta_r = \frac{JV}{304} \exp\left[-m\left(\frac{\delta/d}{K} - \frac{n}{K}\right)\right] \tag{25}$$

$$\frac{\delta/d}{K} = 1.04 \times 10^{-2} V^{2/3} + 4.39 \times 10^{-4} V \tag{26}$$

Equation 26 is substituted into Eq. 25 for $(\delta/d)/K$. If $J = 4$, $m = 3.6$, and $n/K = 2.6$, the curve shown on Fig. 21 results; below 415 ft/sec, $(\delta/d)/K < 2.6$ and the exponential term in Eq. 25 is 1.0. The prediction curve of Eq. 25 correlates well with the experimental data. Figure 22 is a plot of the prediction curves of Eq. 25 for various values of impact obliquity. This figure shows the predictions of the ricochet model for the impact conditions of the test data shown in Fig. 21. It illustrates the effect of impact obliquity upon ricochet obliquity.

The proportionality constant, J, is inversely related to the ratio of the actual elastic energy which appears in the projectile to the maximum which could appear; $J = 4$ is probably a good value for any ricochet situation concerning a solid steel projectile. The constant m governs the rate of decay of the exponential, and there is no reason to believe that its value would be different for different materials. The constant n/K is the value of $(\delta/d)/K$ where plate deflection (deformation and flexure) begins to affect the ricochet obliquity. Though K is dimensionless, there is no justification for presuming that it will be the same for all ricochet impacts (it probably varies with the strength, bulk modulus, and density of the plate). Further, the coefficient 0.29 in Eq. 22 relates to the experiments described herein which involved rigid projectiles. While the model appears to be capable of general application to ricochet predictions, additional data will have to be analyzed to determine how the empirical constants vary.
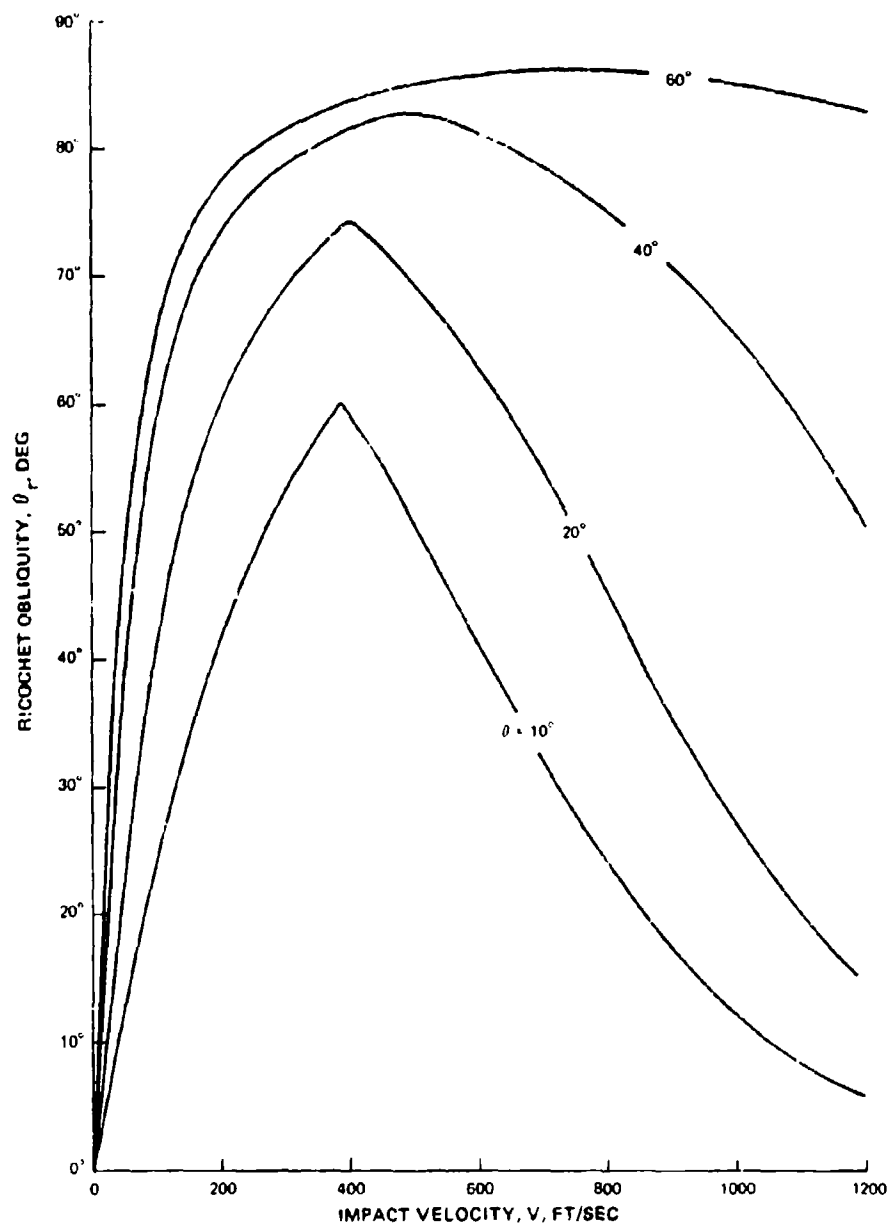
FIG. 22. Ricochet Obliquity as a Function of Impact Velocity as Predicted by Eq. 25.

SUMMARY

Nose shape of rigid penetrators affects ballistic limit velocity and residual velocity as regards the penetration of steel plates. Nose shape has little effect upon ricochet obliquity. The variation in ballistic limit velocity with change in nose shape is not large. Rigid projectiles can be categorized in behavior as "sharp" or "blunt." The classification of a given nose-shaped projectile as to mode of behavior is accomplished by comparing the equivalent conical nose half-angle to the critical nose half-angle. The critical nose half-angle is predictable by analytical methods. Blunt-nosed rigid penetrators behave quite differently from non-rigid penetrators. Based upon the experimental data generated in this program for rigid blunt penetrators, prediction models were successfully modified to provide means of accurately predicting ballistic limit velocity and residual velocity for rigid projectiles having various nose shapes. A model was developed for predicting ricochet obliquity for rigid projectiles and steel plate.

REFERENCES

1. Naval Weapons Center. *Transformation of Terminal Ballistic Threat Definitions into Vital Component Malfunction Predictions*, by R. F. Recht, T. W. Ipson, and E. Wittrock, Denver Research Institute. China Lake, Calif., NWC, May 1969. (NWC TP 4871, publication UNCLASSIFIED.)

2. ------. *Terminal Ballistics of Elongated Fragments*, by T. W. Ipson, and W. A. Schmeling, Denver Research Institute. China Lake, Calif., NWC, December 1972. (NWC TP 5449, publication UNCLASSIFIED.)

3. ------. *Ballistic Penetration of Ship Structure, Final Report* (U), by R. F. Recht, Denver Research Institute. China Lake, Calif., NWC, September 1972. (NWC TP 5419, publication CONFIDENTIAL.)

4. Naval Proving Grounds. *The Construction of Plate Penetration Charts or Tables*, by A. V. Hershey. Dahlgren, Virginia, NPG, May 1955. (NPG Report 1120, publication UNCLASSIFIED.)

5. Denver Research Institute, University of Denver. *The Dynamics of Terminal Ballistics* (U), by R. F. Recht and T. W. Ipson. Denver, Colorado, DRI, February 1962. (Final Report, Contract DA-23-072-ORD-1302, for Army Tank Automative Center; DDC File No. AD-274-128 and AD-328-796; UNCLASSIFIED Report and CONFIDENTIAL Appendix.)

6. Naval Weapons Center. *Characteristics of the Deformation of Ballistically Impacted Waveguide*, by T. W. Ipson and W. A. Schmeling, Denver Research Institute. China Lake, Calif., NWC, February 1972. (NWC TP 5328, publication UNCLASSIFIED.)

INITIAL DISTRIBUTION

8 Naval Air Systems Command
    AIR-03B (1)
    AIR-03P2 (1)
    AIR-350 (1)
    AIR-350D (1)
    AIR-50174 (2)
    AIR-503 (1)
    AIR-5323 (1)
3 Chief of Naval Operations
    OP-05 (1)
    OP-506F (1)
    OP-722 (1)
3 Chief of Naval Material
    MAT-03R (1)
    MAT-032 (1)
    PM-12, Naval Inshore Project Office, Grenville Eldridge (1)
5 Naval Ordnance Systems Command
    ORD-035D (1)
    ORD-0352 (1)
    ORD-0632 (2)
    ORD-552B (1)
3 Chief of Naval Research, Arlington
    ONR-102 (1)
    ONR-420 (1)
    ONR-461 (1)
1 Commandant of the Marine Corps (Code AAW1)
4 Marine Corps Development and Education Command, Quantico
    Marine Corps Educational Center (1)
    Marine Corps Landing Force Development Center, MCTEC (1)
    War Games Division, Marine Corps Landing Force Development Center (1)
    Technical Library (1)
1 Naval Intelligence Support Center (Technical Library)
1 Naval Missile Center, Point Mugu (Technical Library)
7 Naval Ordnance Laboratory, White Oak
    Code 0431 (1)
    Code 045, Jack Wack (1)
    Code 242, T. Liddiard (1)
    Code 244, T. Anderson (1)
    Code 430 (1)
    Code 433, Ralph Craig (1)
    Code 730, Technical Library (1)

1 Naval Postgraduate School, Monterey
1 Naval Research Laboratory
1 Naval Ship Engineering Center, Hyattsville (Code 6105, Ken Lovell)
4 Naval Ship Research and Development Center, Bethesda
    Code 1747, A. B. Willner (1)
    Code 1748, Dr. Fred Fisch (1)
    Code 1749, R. H. Fortune (1)
    Technical Library (1)
1 Naval Undersea Center, San Diego (Code 133)
5 Naval Weapons Laboratory, Dahlgren
    Code GAV
      Jim Logan (1)
      Steve Hock (1)
      Tom McCants (1)
      Wally Morton (1)
    Code MAL, Technical Library (1)
1 Office Chief of Research & Development (CRDCM)
2 Army Combat Developments Command, Fort Belvoir
    CDCMR-U (1)
    CDCSA, Mr. Hardison (1)
1 Army Combat Development Command, Fort Sill (Artillery Agency)
3 Army Materiel Command (RD)
    TE (1)
    W (2)
1 Army Missile Command, Redstone Arsenal
1 Army Munitions Command, Dover (AMSMU-Re R)
4 Army Tank-Automotive Command, Warren
    AMOTA-TRS.2, R. Nadler (2)
    SMOTA-RCM, V. Pagona (1)
    SMOTA-RCM.1, H. Spiro (1)
1 Army Weapons Command, Rock Island Arsenal (Technical Library)
1 Headquarters, U. S. Army Europe (AEUTTIC, Technical Intelligence Center)
2 Aberdeen Research & Development Center, Aberdeen Proving Ground
    STEAP-1, Foreign Technical Intelligence Office (1)
    Technical Library (1)
5 Army Ballistics Research Laboratories, Aberdeen Proving Ground (AMXRD)
    BEL-FT, C. Lebegern (1)
    BTL, Dr. Cc/ Glass (1)
    BVL
      M. Bernier (1)
      Mr. Vikestad (1)
      Mr. Hoffman (1)
1 Army Engineer School, Fort Belvoir (Technical Library)
1 Army Land Warfare Laboratory, Aberdeen Proving Ground (Technical Library)
2 Army Materiel Systems Analysis Agency, Aberdeen Proving Ground (AMXSY)
    D, Dr. Sperrazza (1)
    S, J. Kramar (1)

3 Army Materiels and Mechanics Research Center, Watertown
   Robert Frost (1)
   Tony Alesi (1)
   Technical Library (1)
2 Edgewood Arsenal (SMUEA)
   TSS-OA, Mr. Schroeter (1)
   TSTI-L (1)
1 Foreign Science & Technology Center (Technical Library)
3 Franktord Arsenal
   SMUFA
      C2500 (1)
      U3200 (1)
   Harold Markus (1)
3 Picatinny Arsenal
   SMUPA
      AD-C-S, J. Killen (1)
      DW6, G. Gaydos (1)
   Technical Library (1)
1 Air Force Logistics Command, Wright-Patterson Air Force Base (MMWM,
E. C. Swanson)
2 Air Force Systems Command, Andrews Air Force Base
   SCFO (1)
   SDW (1)
2 Tactical Air Command, Langley Air Force Base
   DIT (1)
   OA (1)
3 Aeronautical Systems Division, Wright-Patterson Air Force Base
   Code AFFDL, Vulnerability Group, Don Voyls (1)
   Code XRHD, G. Bennett (1)
5 Air Force Armament Laboratory, Eglin Air Force Base
   DLRV
      C. Crews (1)
      J. A. Collins (1)
      J. B. Flint (1)
   DLYW, Marvis Adams (1)
   Oklahoma State University Detachment, R. H. Armstrong (1)
1 Air Force Weapons Laboratory, Kirtland Air Force Base (WLDC)
1 Air University Library, Maxwell Air Force Base (Document Library)
1 Armament Development & Test Center, Eglin Air Force Base
2 Foreign Technology Division, Wright-Patterson Air Force Base
   TDFAD (1)
   Technical Library (1)
1 Tactical Fighter Weapons Center, Nellis Air Force Base (Code C-OA)
1 Director of Defense Research & Engineering (Technical Library)
1 Assistant Secretary of Defense (Systems Analysis)
2 Defense Advanced Research Projects Agency, Arlington (Technical
Information Center)
12 Defense Documentation Center

DOCUMENT CONTROL DATA - R & D

Security classification of title, body of abstract and indexing annotation must be entered when the overall report is classified)

1. ORIGINATING ACTIVITY (Corporate author)	2a. REPORT SECURITY CLASSIFICATION
Denver Research Institute University of Denver Denver, Colorado	UNCLASSIFIED
	2b. GROUP

3. REPORT TITLE

Effect of Projectile Nose Shape on Ballistic Limit Velocity, Residual Velocity, and Ricochet Obliquity

4. DESCRIPTIVE NOTES (Type of report and inclusive dates)

5. AUTHOR(S) (First name, middle initial, last name)

Thomas W. Ipson
Rodney F. Recht
William A. Schmeling

6. REPORT DATE	7a. TOTAL NO. OF PAGES	7b. NO. OF REFS
December 1973	38	6

8a. CONTRACT OR GRANT NO	9a. ORIGINATOR'S REPORT NUMBER(S)
N00123-69-C-1970	
b. PROJECT NO	NWC TP 5607
AirTask A-350-5321/008B/3F32-353-501	
c.	9b. OTHER REPORT NO(S) (Any other numbers that may be assigned this report)
d.	

10. DISTRIBUTION STATEMENT

Distribution limited to U. S. Government agencies only; test and evaluation;
14 December 1973. Other requests for this document must be referred to the Naval
Weapons Center.

11. SUPPLEMENTARY NOTES	12. SPONSORING MILITARY ACTIVITY
	Naval Weapons Center China Lake, Calif. 93555

13. ABSTRACT

Target vulnerability analyses consider ballistic penetrators which have various
nose shapes. Nose shape often undergoes changes during the target penetration
process due to deformation. It is important that the effects of nose shape upon
ballistic perforation dynamics be known and accounted for in vulnerability analyses.
An experimental firing program was conducted in which rigid penetrators having three
different nose shapes were fired against steel plate. Experimental data generated
concerned ballistic limit velocity, residual velocity, and ricochet obliquity.
Experimental data were compared with predictions of analytic models. The prediction
models were modified to reflect the results of experiments.

DD FORM 1473 (PAGE 1)

S/N 0101-807-6801

14 KEY WORDS	LINK A		LINK B		LINK C	
	ROLE	WT	ROLE	WT	ROLE	WT
Terminal ballistics						
Experimental data						
Nose shape						
Ballistic limit velocity						
Residual velocity						
Ricochet obliquity						
Ship penetration model						
Vulnerability analysis						
Ballistic prediction models						

Naval Weapons Center
   Effect of Projectile Nose Shape on Ballistic Limit Velocity, Residual Velocity, and Ricochet Obliquity, by Thomas W. Ipson, Rodney F. Recht and William A. Schmeling. Denver Research Institute. China Lake. Calif.. NWC. December 1973. 38 pp. (NWC TP 5607. publication UNCLASSIFIED.)
   Target vulnerability analyses consider ballistic penetrators which have various nose shapes. Nose shape often undergoes changes during the target penetration process due to deformation. It is important that the effects of nose shape upon ballistic perforation dynamics be known and accounted for in vulnerability analyses. An experimental firing program was conducted in which rigid penetrators having three different nose shapes were fired against steel plate. Experimental data generated concerned ballistic limit velocity, residual velocity, and ricochet obliquity. Experimental data were compared with predictions of analytic models. The prediction models were modified to reflect the results of experiments.

1 card, 8 copies

Naval Weapons Center
   Effect of Projectile Nose Shape on Ballistic Limit Velocity, Residual Velocity, and Ricochet Obliquity, by Thomas W. Ipson, Rodney F. Recht and William A. Schmeling. Denver Research Institute. China Lake. Calif.. NWC. December 1973. 38 pp. (NWC TP 5607. publication UNCLASSIFIED.)
   Target vulnerability analyses consider ballistic penetrators which have various nose shapes. Nose shape often undergoes changes during the target penetration process due to deformation. It is important that the effects of nose shape upon ballistic perforation dynamics be known and accounted for in vulnerability analyses. An experimental firing program was conducted in which rigid penetrators having three different nose shapes were fired against steel plate. Experimental data generated concerned ballistic limit velocity, residual velocity, and ricochet obliquity. Experimental data were compared with predictions of analytic models. The prediction models were modified to reflect the results of experiments.

1 card, 8 copies

ABSTRACT CARD

Naval Weapons Center

Effect of Projectile Nose Shape on Ballistic Limit Velocity, Residual Velocity, and Ricochet Obliquity, by Thomas W. Ipson, Rodney F. Recht and William A. Schmeling. Denver Research Institute. China Lake, Calif., NWC, December 1973. 38 pp. (NWC TP 5607, publication UNCLASSIFIED.)

Target vulnerability analyses consider ballistic penetrators which have various nose shapes. Nose shape often undergoes changes during the target penetration process due to deformation. It is important that the effects of nose shape upon ballistic perforation dynamics be known and accounted for in vulnerability analyses. An experimental firing program was conducted in which rigid penetrators having three different nose shapes were fired against steel plate. Experimental data generated concerned ballistic limit velocity, residual velocity, and ricochet obliquity. Experimental data were compared with predictions of analytic models. The prediction models were modified to reflect the results of experiments.

1 card, 8 copies

Naval Weapons Center

Effect of Projectile Nose Shape on Ballistic Limit Velocity, Residual Velocity, and Ricochet Obliquity, by Thomas W. Ipson, Rodney F. Recht and William A. Schmeling. Denver Research Institute. China Lake, Calif., NWC, December 1973. 38 pp. (NWC TP 5607, publication UNCLASSIFIED.)

Target vulnerability analyses consider ballistic penetrators which have various nose shapes. Nose shape often undergoes changes during the target penetration process due to deformation. It is important that the effects of nose shape upon ballistic perforation dynamics be known and accounted for in vulnerability analyses. An experimental firing program was conducted in which rigid penetrators having three different nose shapes were fired against steel plate. Experimental data generated concerned ballistic limit velocity, residual velocity, and ricochet obliquity. Experimental data were compared with predictions of analytic models. The prediction models were modified to reflect the results of experiments.

1 card, 8 copies

---

3 Defense Intelligence Agency
    DI-7, COL A. Belmont (1)
    DI-7E, MAJ N. L. Leone (1)
    Technical Library (1)
1 Center for Naval Analyses, University of Rochester, Arlington, Va.
1 Falcon Research & Development Company, Albuquerque, New Mexico
1 Falcon Research & Development Company, Baltimore, Md.
1 Falcon Research & Development Company, Denver, Colo.
1 Honeywell Inc., Systems & Research Division, Minneapolis, Minn.
    (C. R. Hargreaves)
2 Institute for Defense Analyses, Arlington, Va.
    Research & Engineering Division (1)
    Technical Library (1)
2 Remote Area Conflict Information Center, Battelle Memorial Institute,
    Columbus, Ohio
1 Rockwell International Corporation, Los Angeles, Calif. (W. L. Jackson)
1 The Boeing Company, Seattle, Wash. (R. G. Blaisdell)
3 University of Denver, Denver Research Institute, Denver, Colo.
    T. W. Ipson (1)
    R. F. Recht (1)
    W. A. Schmeling (1)